VERIFICATION DOCUMENT FOR

ULTRAMARINE OFFSHORE SOFTWARE

Phone (713) 975-8146 Fax (713) 975-8179

Contents

I. INTRODUCTION

The purpose of this document is to provide information on the applicability of the results produced by Ultramarine's software, MOSES, to "real world" problems. We begin by considering some simple problems where exact solutions are available. Many problems of interest, however, are not amenable to such checks. For these cases, we turn to comparisons with model tests and/or other computed results.

Although not strictly applicable, it should be mentioned that MOSES has been around in some incarnation since the late 1970's and it has been used on hundreds of projects. This is, perhaps, the best statment for the accuracy and reliability of the results it produces.

Because of the range of problems our software can solve, it is impossible to compare everything. What we have here are enough comparisons to establish that the "basic ingredients" function properly. Thus, they give comfort that MOSES functions properly for a much wider class of problem than covered here.

The document finishes with a description of our Quality Assurance procedures. In essence, these procedures are designed to minimize the chance of errors creeping into the software during the maintenance process.

II. REGULARATORY APPROVAL

One of the questions we are continually asked about is whether or not MOSES is approved by some regulatory bodies such as ABS or DNV. The answer to this is **no**, regulatory bodies, in general, approve result and designs, not software. Since MOSES has been in constant use for decades, literally hundreds of results have been approved by various regulatory bodies. Never have we heard of a case where a design or analysis was rejected because of the software used.

One exception that we know of to the above rule is that the Norweign Petroleum Directoriat did (or does) approve combinations of organizations and software to perform mooring and stability calculations. There are several organizations - MOSES combinations which have been aproved.

III. PERIODIC MOTION

In this section we investigate two cases of periodic motion which can be compared with exact solutions. A simple spring-mass system is considered first, and then we look at the large motion of a pendulum. The primary objective is to examine how well time domain problems can be solved. In particular, is appreciable numerical damping induced into the solution, and are the nonlinearities properly accounted for. The two samples chosen also address the question of how well flexible and rigid connections function in the time domain.

The first test consists of a spring, modeled by a vertical bar with a Young's modulus of 10 kips/in^2, length of 100 ft., and a constant circular cross section of 1 ft. diameter. The block has a weight of 1000 kips as is shown in Figure 1. To initiate the motion, the mass was displaced by 10 ft. in the positive z-direction and released.

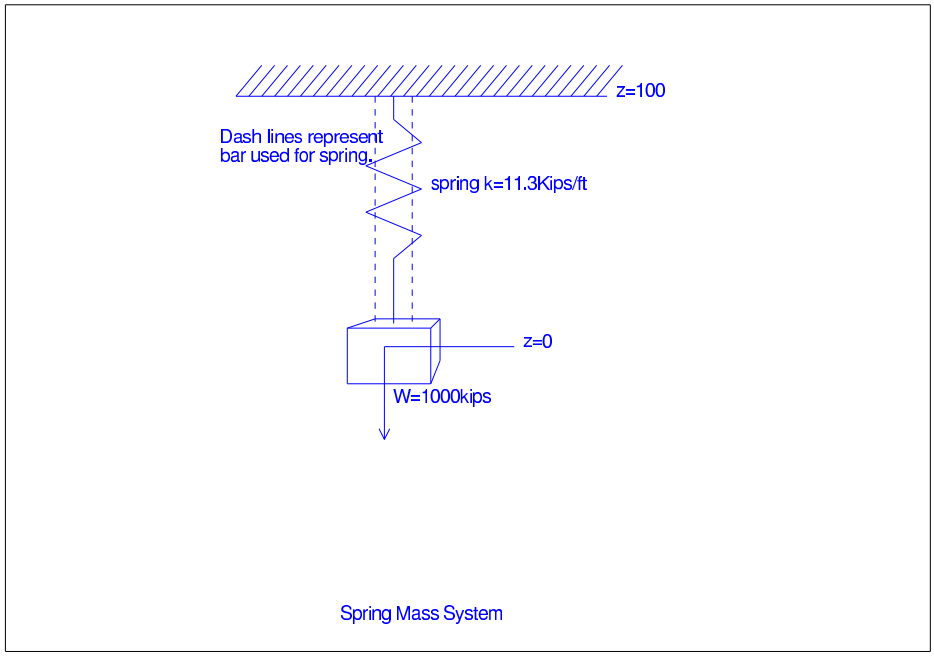

Figure 1: Setup for Spring Vibration

For uniaxial deformation, the deflection of the bar under load P is

$$\delta = \frac{PL}{AE}, \tag{III.1}$$

and the spring constant is

$$k = \frac{P}{\delta} = \frac{AE}{L}. \tag{III.2}$$

The quantities verified are the natural frequency, the force needed to stretch the spring 10 ft., and the stretched length of the spring with a 1000 kip block. The force required to change the length of the bar 10 ft. can be determined by solving (III.1) for P,

$$P = \frac{\delta EA}{L} \tag{III.3}$$

which for a $\delta = 10$ft and the bar particulars given above results in $P = 113.09$ Kips. The natural frequency and period of the system are given by

$$\omega_n = \sqrt{\frac{k}{m}}, \text{ and} \tag{III.4}$$

$$T = \frac{2\pi}{\omega_n}. \tag{III.5}$$

Using these equations with the spring constant of 11.3 kips/ft given by (III.2) yields a natural period of 10.37 sec. The stretched length of the spring corresponds to the average length of the spring during oscillation. In Figure 2 we show the mean oscillation being about z=-89 ft. Recalling that the spring is 100 ft. long at z=0 ft. will conclude that the springs stretched length is 189 ft. Again using (III.1) with the weight of the block gives the stretched length of the bar to be 88.5 ft. from its z=0 ft. position.

Below we present the comparison of hand calculated values to those from MOSES. As can be seen there is a good comparison between the force needed to move the block to z=10 ft., the natural period, and the stretched length. The force to move the block to z=10 ft. was taken from the MOSES status report, the mean z-location was taken from the statistics of the block motion, and the natural period was taken from the plot of oscillatory motion for 100 sec. Finally, notice that the numerical integration did not induce any perceptible error.

Comparison of Exact Solution and MOSES for Spring-Mass System

Quantity	units	Hand	MOSES
Force to move to z=10 ft.	kips	113.00	113.00
Natural period	sec.	10.41	10.40
Z-Mean	ft.	88.50	88.42

Next we consider the large angular motion of a pendulum. This is by far the more interesting of the two tests, since the governing equation is nonlinear. The system

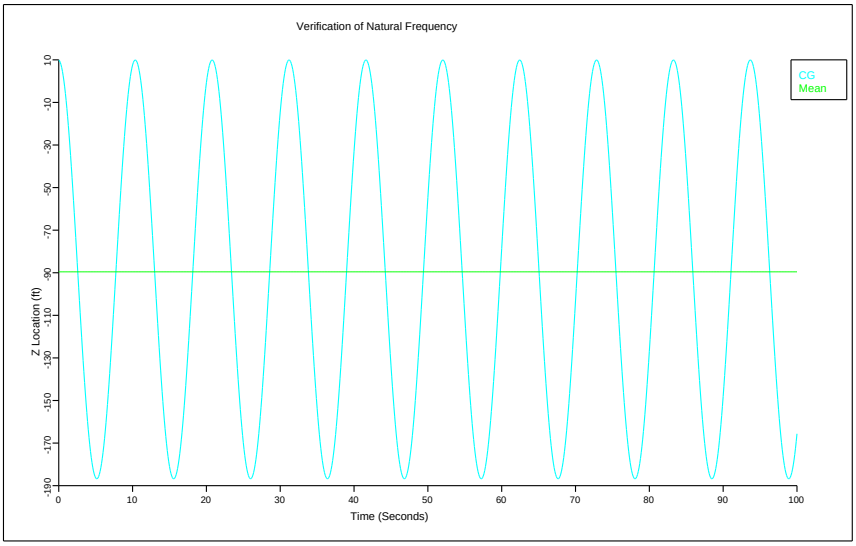

Figure 2: Vibration of Spring-Mass System

consists of a 100 ft. bar of constant section, hinged at one end. The bar is initially rotated 90 degrees and released.

The equation of motion for the pendulum in terms of the angle, θ, mass, m, length of bar, l, and moment of inertia, I_o is

$$\ddot{\theta} + \omega^2 \sin\theta = 0 \ , \tag{III.6}$$

where

$$\omega^2 = \frac{3g}{2l}, \tag{III.7}$$

and g is the acceleration of gravity. The period for motion satisfying this equation is an elliptic integral and can be represented as

$$T = \frac{2}{\pi} K(2\pi\omega) \tag{III.8}$$

where K is dependent on the initial amplitude. For 90 degrees $K = 1.854$ which yields a period of $T = 10.66$ sec. As can be seen from Figure 3 the computed results have a period which is the same as the predicted value. It is also worth noting the plateaus in the acceleration vs. time plot shown in Figure 4. The motion here is certainly not described by a cosine.

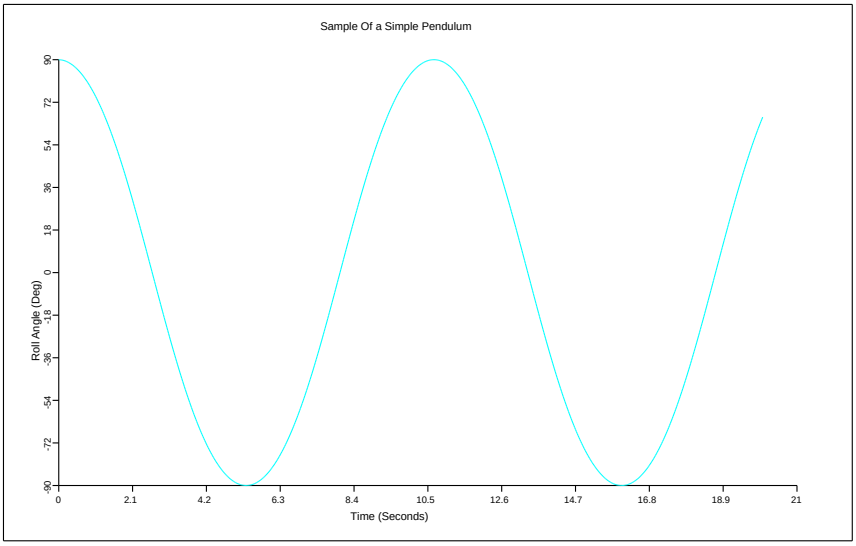

Figure 3: Oscillation of Pendulum Motion

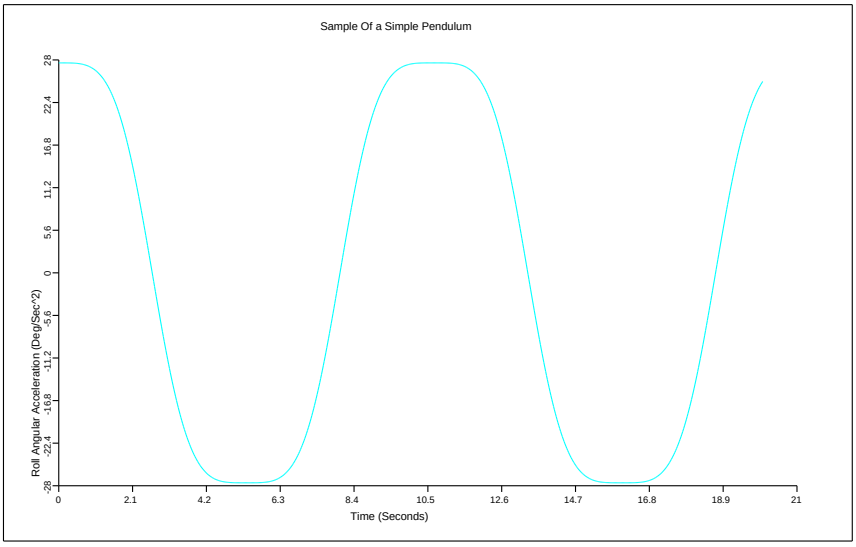

Figure 4: Acceleration of Pendulum Motion

IV. PLATE DEFORMATION

In this section we consider the deformation of a cantelever plate due to uniaxial loading and pure bending. The deformation of the cantelever is simple enough so that MOSES results can be easily compared. We considered three plate models. In all three models the main dimensions of the cantelever remained the same, however the refinement of the sections considered was changed. This example not only illustrates how the plate element is used, but demonstrates how accuracy is increased with detail.

There were three models considered: a single plate, a plate refined along the y-axis, and a plate refined along both the y-axis and the x-axis. For all three cases there was an axial force in the negative x-direction, a shear load in the negative z-direction and a shear load in the negative y-direction. These three cases are shown in Figure 5. The dimensions of the plate are length of 10 ft., width of 4 ft., and thickness of 1 in.

The equations that govern the deformation of the plate are:

$$\begin{aligned} \delta_x &= \frac{f\ell}{EA} \ , \\ \delta_y &= \frac{P\ell^3}{3EI_{yy}} \ , \\ \delta_z &= \frac{P\ell^3}{3EI_{zz}} \ , \end{aligned} \tag{IV.1}$$

where

$$\begin{aligned} A &= wt \ , \\ I_{yy} &= \frac{tw^3}{12} \ , \text{ and} \\ I_{zz} &= \frac{wt^3}{12} \ . \end{aligned} \tag{IV.2}$$

The comparison of MOSES values to hand calculated values is shown in below. An important thing to notice about these results is the dramatic improvement of δ_y with refinement. A single plate element is simply incapable of representing global bending due to membrane stresses.

Plate Deformation with Different Models

	Hand Calculations	MOSES Uniform	MOSES Sliced	MOSES Diced
δ_x (in.)	0.086	0.086	0.086	0.087
δ_y (in.)	0.215	0.058	0.162	0.235
δ_z (in.)	4.966	4.646	4.928	4.768

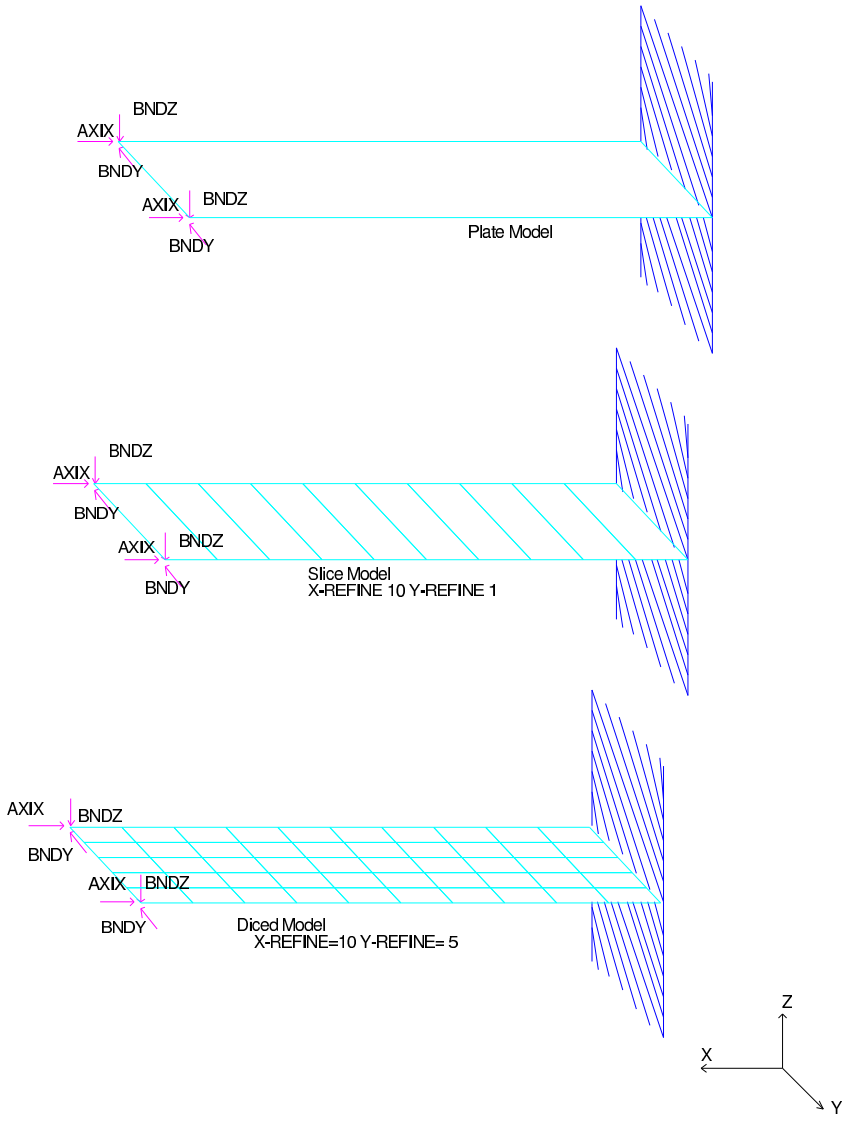

Figure 5: Plate refinement models

V. HOOP STRESS IN A CYLINDER

In this section, we will investigate how well MOSES computes the hoop stresses in a thin-walled cylindrical shell due to external pressure. Here, we consider a cylinder with the radius r=31.5 ft., thickness t=1 in., and total length ℓ= 300 ft. The cylinder was submerged 295 ft. with no trim or heel.

Since MOSES employs a finite element method, the answer will depend on how accurately we model the cylinder. Thus, results for four models were obtained: two models with the nodes on the perimeter of the cylinder and two with a distance from the center that preserves the area. For each scheme of placing the nodes, models of 8 and 16 plates around the circumference were created. Plots of the modes are shown below. Notice that to preserve the area, a different distance is needed for each number of plates:

$$d = \sqrt{\frac{2\pi r^2}{n \sin(\frac{2\pi}{n})}}$$

For the r we have, this corresponds to d=33.2 ft. for 8 plates and d=31.91 ft. for 16 plates. Figures 6 through 8 show the geometric difference in detail.

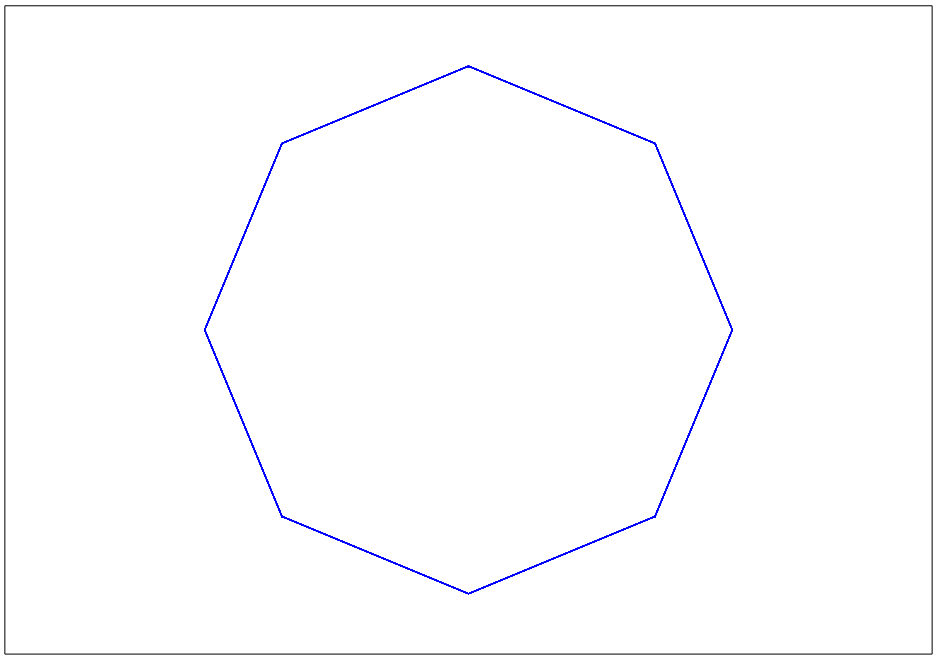

Figure 6: Top View of Simple Models

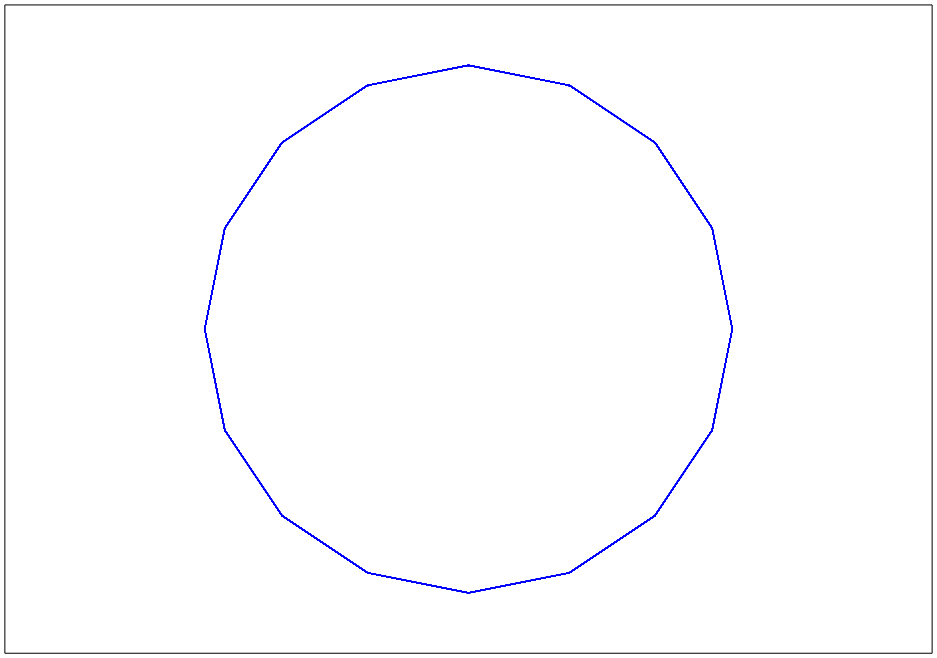

Figure 7: Top View of Detail Models

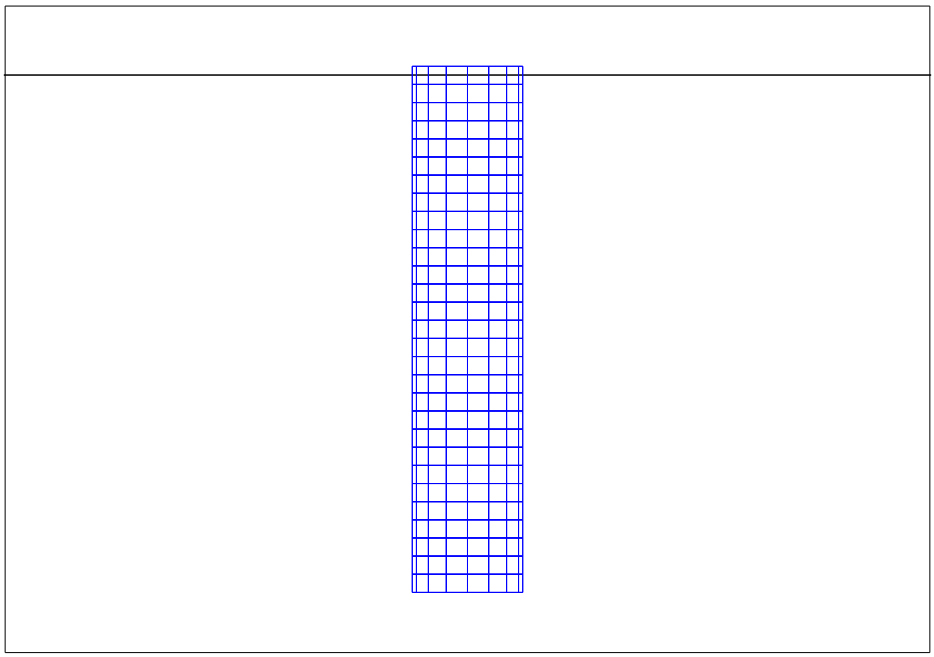

Figure 8: Side View of Detail Models

The "standard results" are given by:

$$\begin{aligned} \sigma_r &= 0 \ , \\ \sigma_\theta &= \frac{Pr}{t} \ , \\ \sigma_z &= \frac{Pr}{2t} \ , \\ P &= -\rho g h \ . \end{aligned} \tag{V.1}$$

Here, σ_r is the radial stress, σ_θ is the tangential stress, σ_z is the longitudinal stress, r is the inner radius, t is the shell thickness, P is the pressure, ρ is the density of water, g is the gravitational constant, and h is the water depth of the point being measured.

Membrane Stess of a Thin Walled Cylindrical Shell

	σ_θ	σ_z
Standard Formulae	-49.35	-24.68
8 Plates on Perimeter	-43.93	-21.37
8 Plates Preserve Area	-46.28	-22.52
16 Plates on Perimeter	-47.65	-23.49
16 Plates Preserve Area	-48.26	-23.80

It is interesting that the results for the equivalent area models are substantially better than the ones from the perimeter models. Also, the results are surprisingly close for such crude models.

VI. STRESS CONCENTRATION OF A CIRCULAR HOLE

In this section we consider the stress concentration factor for a circular hole in a plate subjected to "uniform" tension. Figure 9 shows the plates as defined and Figure 10 shows the refined mesh of 2732 nodes which is actually used to solve for the stresses around the hole.

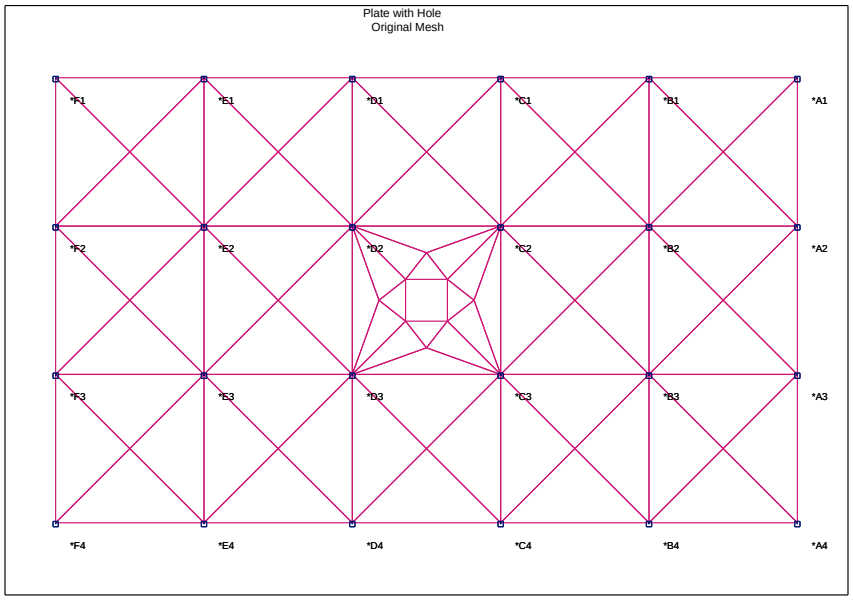

Figure 9: Original Model

Loads are applied to the left edge of the model and the right edge of the model is restrained. The total load applied is 1200 kips and this yields a nominal stress of 3.33 ksi. Figure 11 shows the stress distribution around the hole. The maximim stress here is 9.43 giving a stress concentration factor of 2.83 which compares quite nicely with the correct value of 3.

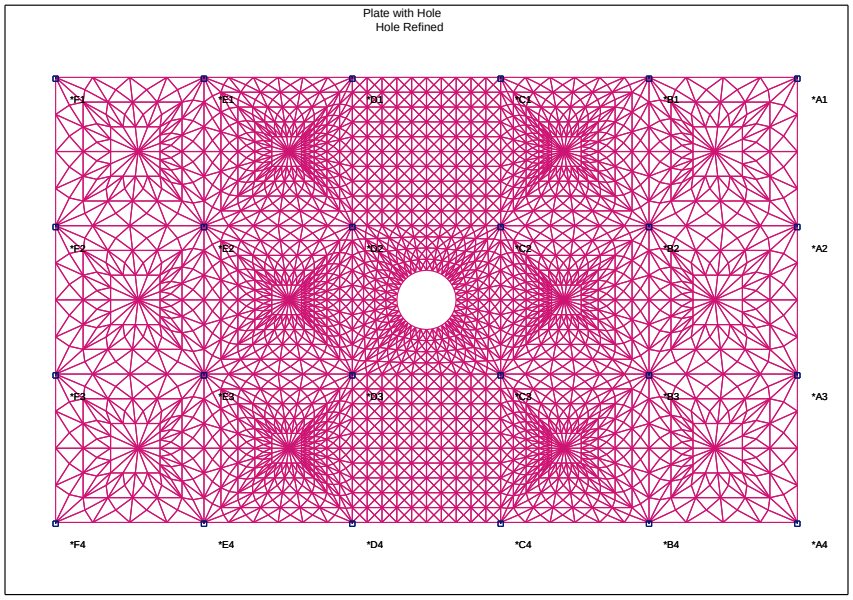

Figure 10: Refined Model

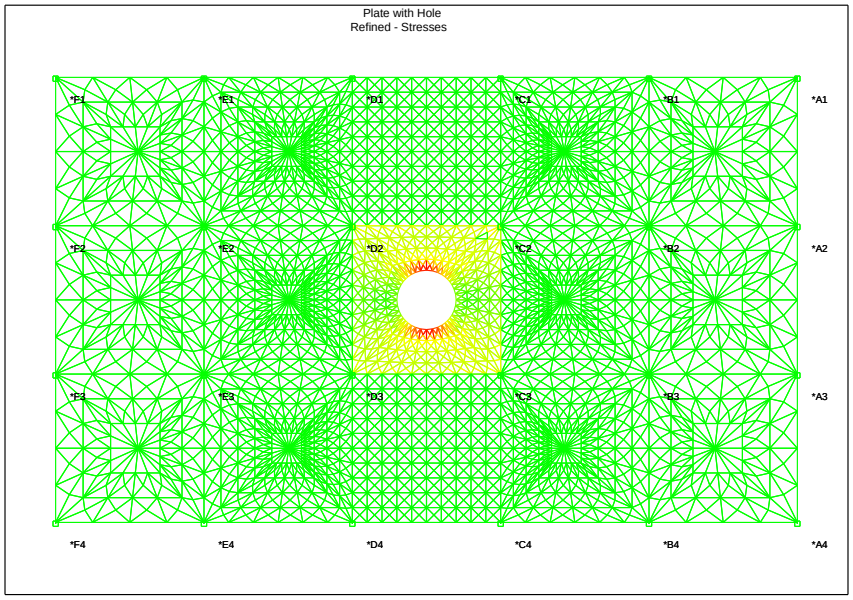

Figure 11: Stress Around Hole

VII. GENERALIZED DEGREES OF FREEDOM

MOSES's generalized degrees of freedom was designed to solve problems that really are not solvable by any other means, and as a result, this capability is not easy to check. Our approach here is to construct an estimate of the solution to a problem, check the estimate where it can be checked, and then compare it with MOSES. In particular, we want to solve a "flag pole", a vertical beam with a weight on top, and we will compare the MOSES results to this problem with a standard energy approximation; i.e. we will look at energy in the beam system:

$$\begin{aligned} K &= \frac{\rho}{2}\int_0^{\ell_1+\ell_2} \dot{x}^2\,dz + \frac{1}{2}\frac{W}{g}\dot{x}(\ell_1+\ell_2)^2\ , \\ V_1 &= \frac{1}{2}EI\int_0^{\ell_1+\ell_2} (x'')^2\,dz\ , \\ V_2 &\approx -\frac{W}{2}\int_0^{\ell_1+\ell_2} (x')^2\,dz \text{ and} \\ W &= \int_0^{\ell_1+\ell_2} F(z)\,x\,dz\ . \end{aligned} \tag{VII.1}$$

Here, the first term of K is the kinetic energy of the beam itself, the second is the kinetic energy of the weight on the top, V_1 is the strain energy due to bending the beam, V_2 is the potential energy due to the weight at the top, and W is the work done by forces acting along the beam. We will consider the beam to be "pinned" at $z = 0$ and $z = \ell_1$, so we really have a two span beam which approximates a cantilever when ℓ_1 is small in comparison to $\ell_1 + \ell_2$.

Now, assume $x(z)$ is a function with continuous derivatives, satisfies the boundary conditions, and depends on a single parameter δ, the value at $z = \ell_1 + \ell_2$. Then

$$\begin{aligned} K &= -\frac{1}{2}(\dot{\delta})^2\left(\rho\int_0^{\ell_1+\ell_2} x^2\,dz + \frac{W}{g}\right) \equiv \frac{1}{2}(\dot{\delta})^2 Mi\ , \\ V_1 &= \frac{1}{2}(\dot{\delta})^2 EI\int_0^{\ell_1+\ell_2} (x'')^2\,dz \equiv \frac{1}{2}(\delta)^2 K_1\ , \\ V_2 &= \frac{1}{2} - (\dot{\delta})^2(W\int_0^{\ell_1+\ell_2} (x')^2\,dz \equiv -\frac{1}{2}(\dot{\delta})^2\frac{1}{2}K_2 \text{ and} \\ W &= \delta\left(F_o + \int_0^{\ell_1+\ell_2} fx^2\,dz\right) \equiv \delta(F_o + C)\ . \end{aligned} \tag{VII.2}$$

Here, F_o is a force applied at the top of the beam and C is a contribution due to a

force, f, acting along the beam.

If we now look at conservation of energy, we get an equation

$$K + V_1 + V_2 = W \tag{VII.3}$$

which, if we use (VII.3) and differentiate with respect to time, yields

$$M\ddot{\delta} + (K_1 - K_2)\delta = F_o + C \ . \tag{VII.4}$$

Now, let us assume that δ, F_o, and C are harmonic in time with frequency ω, which will reduce the above equation to an algebraic one:

$$-\omega^2\delta M + (K_1 - K_2)\delta = F_o + C \tag{VII.5}$$

or

$$\delta = \frac{F_o + C}{[-\omega^2 M + (K_1 - K_2)]} \ . \tag{VII.6}$$

If we have computed the integrals K_1, K_2, C, and M then (VII.6) provides an estimate of the deflection at the top of our beam.

Before attaching the integrals, let us first look at some special cases of verify:1. First, notice that it does not have a solution when

$$\omega^2 = \frac{K_1 - K_2}{M} \tag{VII.7}$$

which gives us an estimate of the natural frequency of the beam. Also, notice that when $C = 0$ and $\omega = 0$, it yields

$$\delta = \frac{F_o}{(K_1 - K_2)} \tag{VII.8}$$

which is the static deflection due to a load applied at the top. These two results will be used to check the accuracy of this approximation. Since (VII.6) has a singularity at the natural period, we will alter it slightly with a bit of damping

$$\delta = \frac{F_o + C}{\sqrt{[-\omega^2 M + (K_1 - K_2)]^2 + 4\eta^2(K_1 - K_2)M}} \ . \tag{VII.9}$$

We are still free to chose any x which satisfies the boundary conditions:

$$\begin{aligned} x(\ell_1) &= 0 \\ \lim_{z\to\ell_1^+} x'(z) &= \lim_{z\to\ell_1^-} x'(z) \\ x''(\ell_1) &= 0 \\ x(\ell_1+\ell_2) &= 1 \\ x''(\ell_1+\ell_2) &= 0\ . \end{aligned} \tag{VII.10}$$

Our choice is the static deflection under a top load:

$$x = \begin{cases} \alpha z + \beta z^3, & z \le \ell_1 \\ \gamma(z-\ell_1) + \psi(z-\ell_1)^2 + \zeta(z-\ell_1)^3, & z > \ell_1 \end{cases} \tag{VII.11}$$

where the parameters α, β, γ, ψ,and ζ can be determined from the above boundary conditions.

The particular problem we consider is a tube with:

$$\begin{aligned} \ell_1 &= 10 \text{ meters}, \\ \ell_2 &= 90 \text{ meters}, \\ W &= 100 \text{ kilo-newtons}, \\ F_o &= 10 \text{ kilo-newtons}, \end{aligned} \tag{VII.12}$$

and which has a diameter of 1 meter and a thickness of 25 millimeters. The buoyancy of the tube was chosen to be equal the weight so that we did not have to include the potential energy of either the weight or the buoyancy of the tube in our equation. When the tube is in the water, the density used above includes both the density of the steel in the tube and the added mass. Also, the integral C is the Morison's equation inertia force due to wave particle acceleration.

Comparing the results of our approximation with the results from a stress analysis we find

Comparison of Energy Approximation with Structural Analysis

Quantity	units	W	Structural	Energy App.
Deflection due to F_o	Meters	0.	1.484	1.484
Deflection due to F_o	Meters	10.	1.484	1.836
Natural period in Air	sec.	0.	.476	.468
Natural period in Water	sec.	0.	12.785	12.920
Natural period in Water	sec.	10.	12.785	14.220

These comparisons are interesting. First, the comparisons with $W = 0$ are excellent, but those for a nonzero weight are not so good. This is due to the fact that the structural analysis we are comparing with is *linear*; i.e. the effect of the weight on the stiffness is not accounted for. Thus, for these cases the estimate is itmore correct than the stress analysis.

Since the estimate is reasonably reliable, we can turn to a comparison of the results from MOSES generalized coordinates and the estimate. We first computed three modes of the beam in water using the pin connections and then used these as generalized coordinates. The following two figures show a comparison of the results both with a weight and without. As you can see, MOSES does quite a nice job of predicting the response *including* the nonlinearities.

One must be a bit careful using generalized coordinates. Above, we had a set of modes which exactly satisfied the boundary conditions. To show what can happen if you do not have a "good set" of modes, we also solved the same problem with a "bad" set of modes. These "bad" modes are backward; i.e. they correspond to a beam fixed at the top! The second set of figures show the results using two of these modes and twenty of them. As you can see, with two modes, you have a really bad estimate of the deformation, while with twenty it is not so bad.

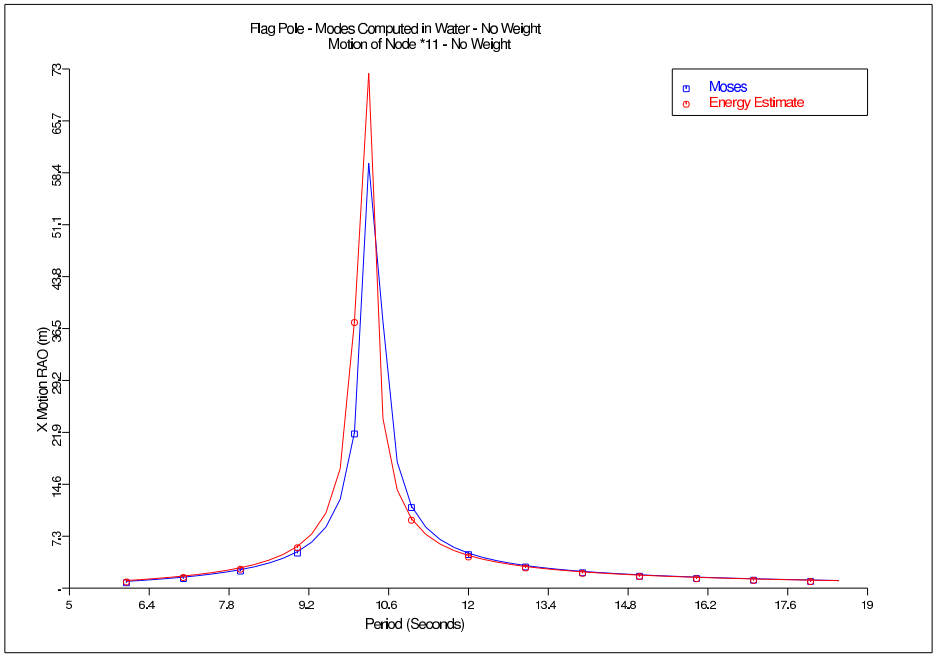

Figure 12: Frequency Response with No Weight

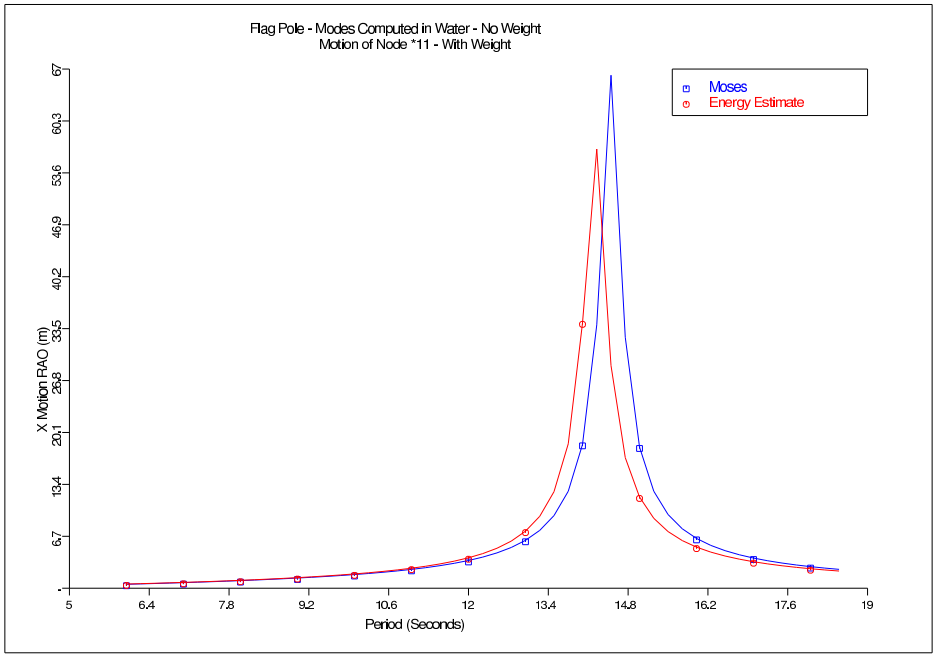

Figure 13: Frequency Response with Weight

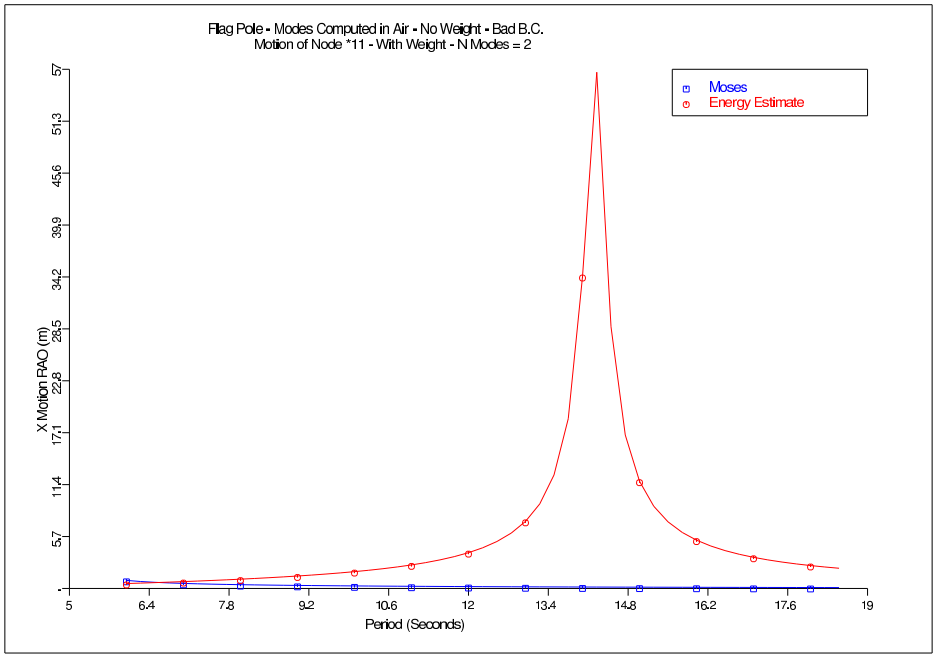

Figure 14: Two "Bad" Modes

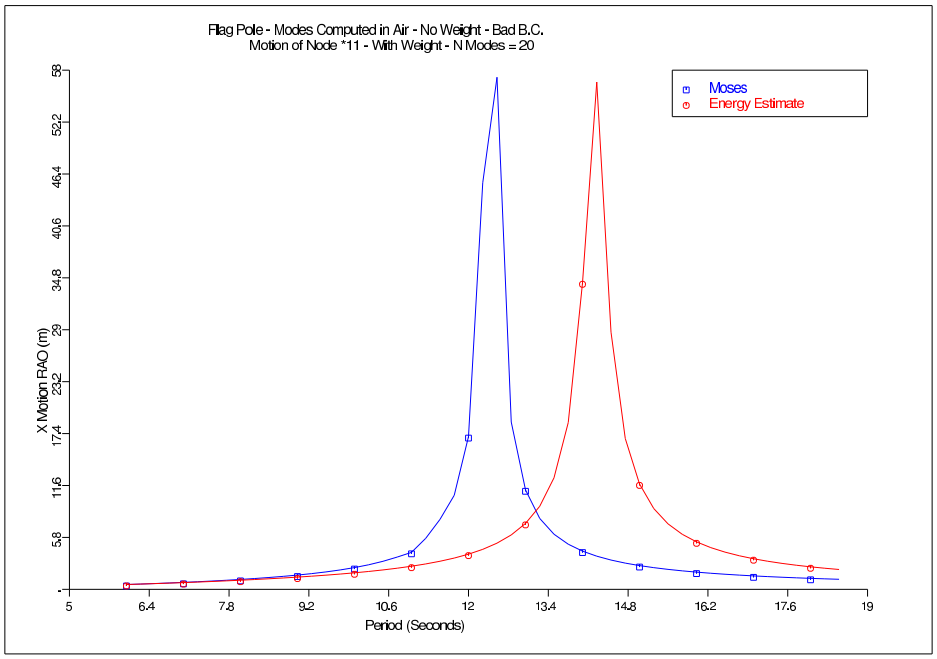

Figure 15: 20 "Bad" Modes

VIII. BEAM RESIZING

In this section we present the beam resizing option. Several examples illustrating how the algorithm works are included as samples of MOSES to show the procedure used for resizing. All resizing samples are taken from classic textbook examples. A brief explanation of each sample follows.

Gaylord and Gaylord, *Design of Steel Structures*, Example 5-12, DP5-2: Crane for shop building. Given the length and the load of the bridge and the girder, determine the size of the beams needed.
Root filename: resiz1

Salmon and Johnson, *Steel Structures Design and Behavior*, Example 15.4.1. Design a rectangular frame of 75-ft. span and 25-ft. height to carry a gravity uniform load of 1.0 kip/ft. when no lateral load is acting.
Root filename: resiz2

AISC *Manual of Steel Construction* beam Examples 1-3, p. 2-5 through 2-6. Design a beam subjected to a given bending moment and a specific compressions flange brace intervals.
Root filename: resiz3

AISC *Manual of Steel Construction* beam Example 1, p. 3-4. Given a concentric load and the effective length with respect to the minor axis, determine the size of the beam needed.
Root filename: resiz4

AISC *Manual of Steel Construction* beam Example 10, p. 2-147. Given the load on a girder, the distance from the ends reaction points, and the moment at the center, determine the girder size.
Root filename: resiz5

The user is asked to use the samples provided and the references to supplement this section of the verification manual.

IX. SIMPLE HYDROSTATICS

In this section, we consider the hydrostatic properties of two simple bodies, a cube and a tube. These bodies are simple enough so that exact calculations can be made, and **MOSES** uses two different algorithms for the two cases. Thus, they provide an excellent check of the hydrostatics for any body.

The cube was considered in three positions: trimmed, heeled, and both trimmed and heeled. The side of the cube has length of $\ell = 50$ft., and a draft T which is measured perpendicular to the waterplane from the deepest submerged point of the body. The equations for the center of buoyancy for the trimmed position and for the heeled position were derived from the center of mass equations of a wedge.

The equations for the center of buoyancy and displacement in a trimmed position are as follows:

$$\begin{aligned} X_{cb} &= \frac{2T}{3\sin\phi} \ , \\ Y_{cb} &= \frac{1}{2}\boldsymbol{l} \ , \\ Z_{cb} &= \frac{T}{3\cos\phi} \ , \text{ and} \\ \Delta &= \rho \boldsymbol{l} \frac{T^2}{\sin 2\phi} \ . \end{aligned} \tag{IX.1}$$

For a heeled position, the equations become:

$$\begin{aligned} X_{cb} &= \frac{1}{2}\boldsymbol{l} \ , \\ Y_{cb} &= \frac{2T}{3\sin\theta} \ , \\ Z_{cb} &= \frac{T}{3\cos\theta}, \text{ and} \\ \Delta &= \rho \boldsymbol{l} \frac{T^2}{\sin 2\theta} \ . \end{aligned} \tag{IX.2}$$

The equations for the center of buoyancy of a trimmed and heeled box are more complicated since two rotations are taking place. It is simple to see that the volume of a cube for a draft, $T \leq \boldsymbol{l} \sin\theta \cos\phi$ which has been rotated about the y-axis by an

angle θ then rotated about the x-axis an angle ϕ will resemble a tetrahedron. The following equations determine the center of buoyancy and the

$$
\begin{aligned}
X_{cb} &= \boldsymbol{l} - \frac{T}{4\sin\phi} \ , \\
Y_{cb} &= \frac{T}{4\cos\phi\cos\theta} \ , \\
Z_{cb} &= \boldsymbol{l} - \frac{T}{4\cos\phi\sin\theta}, \text{ and} \\
\Delta &= \frac{\rho T^3}{(1000)(6)\sin\phi\cos^2\phi\sin\theta\cos\theta} \ .
\end{aligned} \tag{IX.3}
$$

The coordinate systems are shown in Figures 16, 17 and 18. The global coordinate system with its x-y plane on the waterplane is shown as the coordinate system without primes, and the body coordinate system belonging to the cube is shown as the coordinate system with primes.

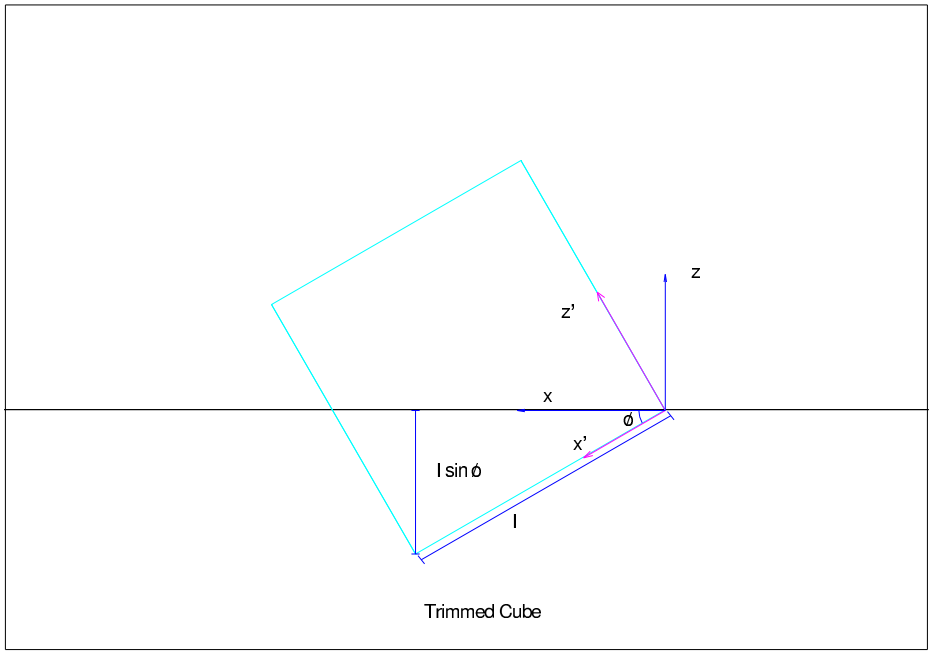

Figure 16: Side View of Cube Position 1

These equations were used to compute the center of buoyancy and the displacement of the cube for the three positions.

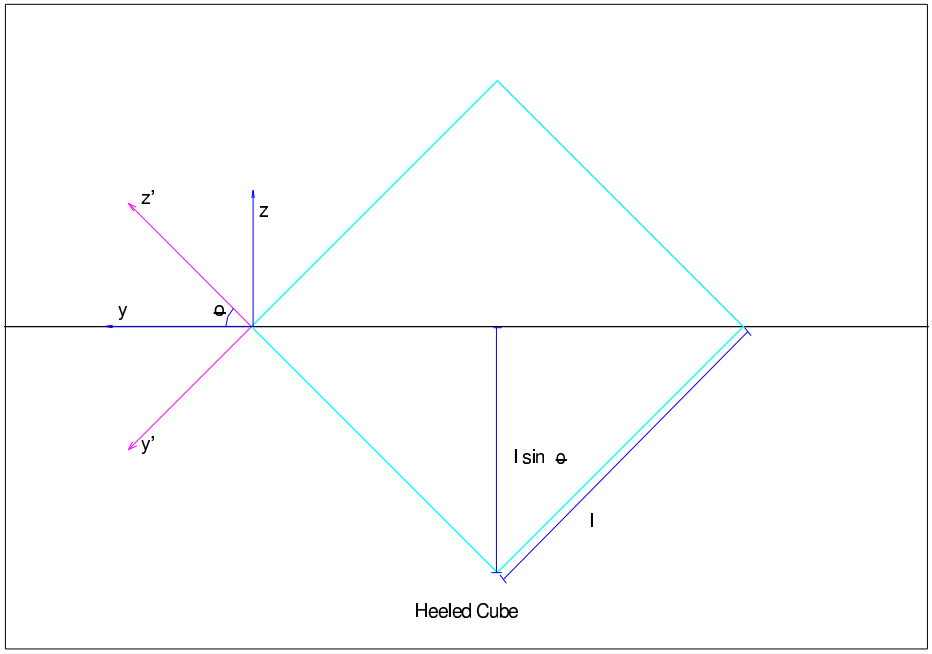

Figure 17: Front View of Cube Position 2

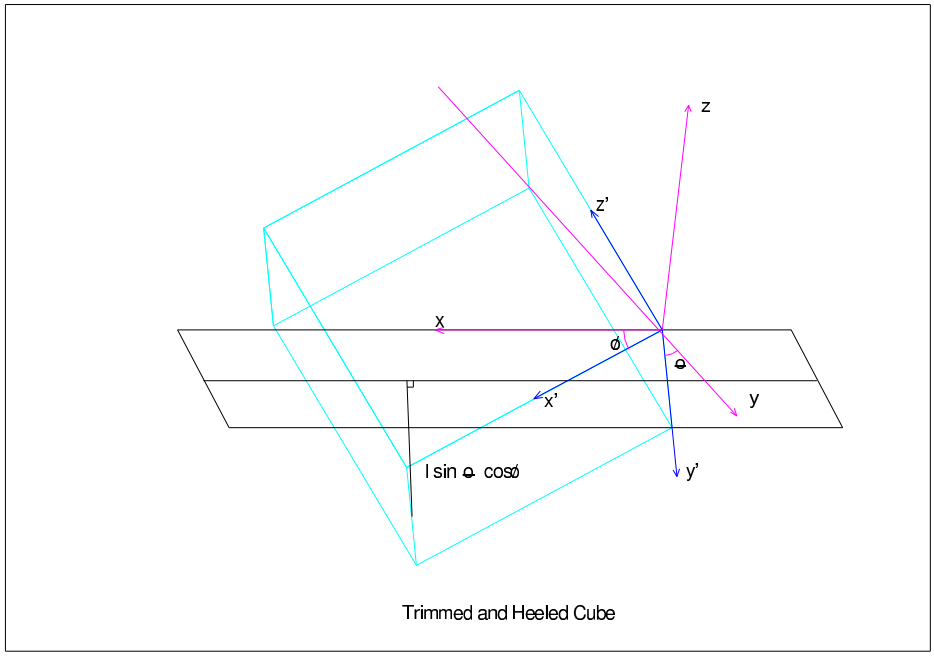

Figure 18: Isometric View of Cube Position 3

Comparison of Hydrostatics of a Cube

Position	Draft ft.	Trim Deg	Roll Deg	Method	Δ Kips	X_{cb} ft.	Y_{cb} ft.	Z_{cb} ft.
1	25.00	30	00	Hand	2309.40	33.33	25.00	9.63
				MOSES	2309.40	33.33	25.00	9.62
2	35.35	00	45	Hand	4000.00	25.00	33.33	16.67
				MOSES	4000.00	25.00	33.33	16.67
3	30.61	30	45	Hand	889.12	37.50	39.79	10.21
				MOSES	889.80	37.50	39.79	10.21

Next, we consider the hydrostatics of a tube in three conditions. The tube is 50 ft. long with a radius of 5 ft. Here θ is a pitch angle measured from the global z-axis to the body z'-axis. For these tests, draft is defined as the vertical distance from the body coordinate system to the mean water level. The geometry is shown in Figure 19, and body coordinate system is denoted as the x'-z' axis.

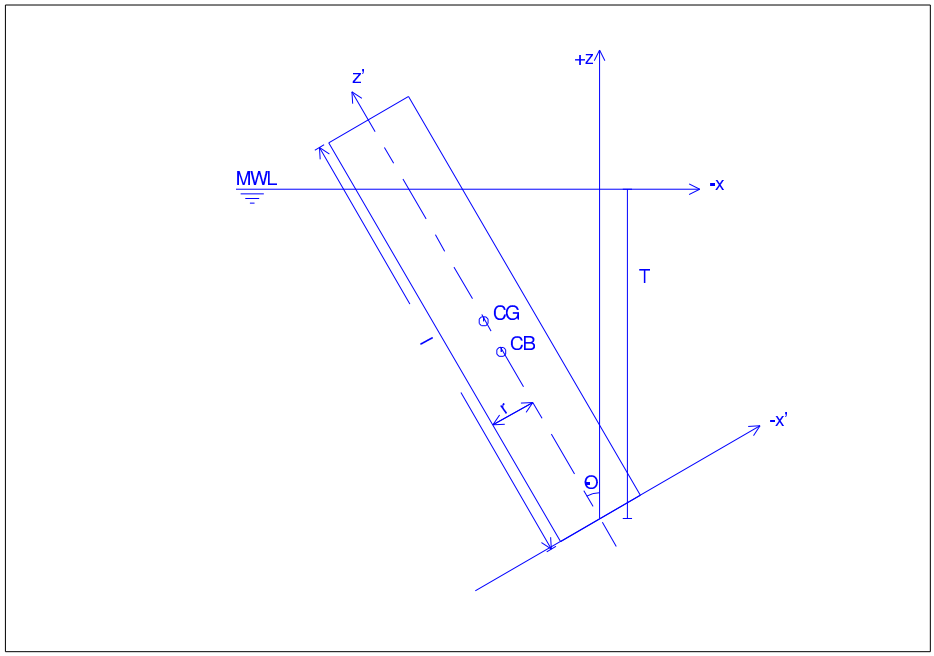

Figure 19: Coordinate System for Buoyancy of a Tube

The buoyancy and its center are determined by integration of the following equations:

$$
\begin{aligned}
v &= \int_S dv \\
\Delta &= \rho g v \\
X_{cb} &= \frac{1}{v}\int_S x\, dv \\
Y_{cb} &= \frac{1}{v}\int_S y\, dv \\
Z_{cb} &= \frac{1}{v}\int_S z\, dv
\end{aligned}
\tag{IX.4}
$$

Here, S is the submerged portion of the tube. The comparison for three cases is:

Comparison of Hydrostatics of a Tube

Position	Draft ft.	Trim Deg	Roll Deg	Method	Δ Kips	X_{cb} ft.	Y_{cb} ft.	Z_{cb} ft.
1	34.64	00	30	Hand	201.09	0.18	0.00	20.09
				MOSES	201.06	0.09	0.00	20.03
2	0.00	60	00	Hand	9.24	2.55	0.00	2.98
				MOSES	9.24	2.50	0.00	2.95
3	0.00	80	00	Hand	30.25	2.92	0.00	8.40
				MOSES	30.25	2.95	0.00	8.35

X. STRIP THEORY HYDRODYNAMICS

In this section, we compare the RAOs of a barge from a study conducted by Noble Denton and Associates Ltd. [1] and those computed by MOSES using strip theory. The model studied is a deck barge of dimensions depicted in Figure 20, with a KG of 32 ft.

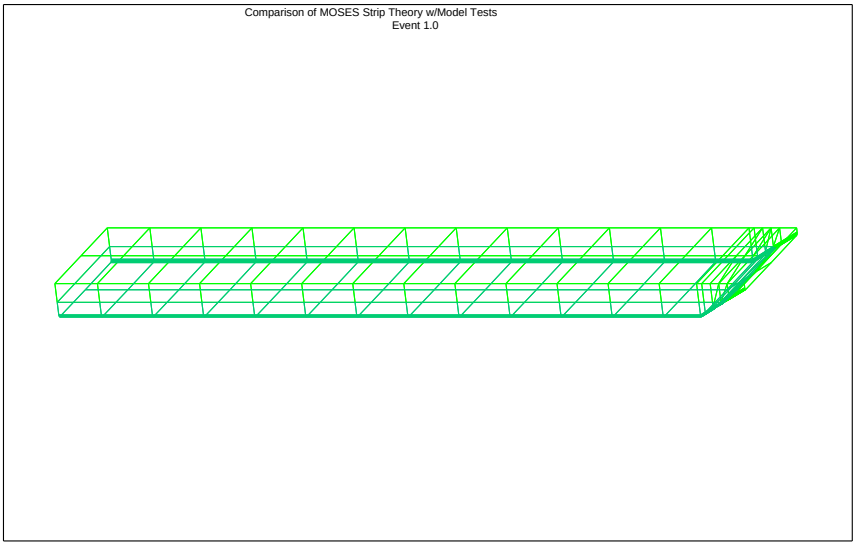

Figure 20: Barge Particulars

The comparisons are shown in Figures 21 to 26. The Noble Denton report consisted of RAO curves with an average of 5 data points per degree of freedom. The data points were from measurements of a 1:30 ratio model in regular waves for head and beam seas. Surge and heave motions were recorded for head seas and sway, heave, and roll motions were recorded for beam seas. The points recorded by Noble Denton are indicated in each curve by circles. Points with a "W" indicate that for this test, the deck of the barge was awash.

The MOSES curves were calculated with a wave steepness of 1/20. As seen from these figures, most of the computed RAOs compare quite well with those from the model test. The only exception is the roll RAOs, in which case the computed results deviate from the test results near resonance. This is due to nonlinear roll damping which causes the response near resonance to be greatly affected by the wave steepness.

To address this nonlinearity, roll response curves were calculated for a range of wave steepnesses. These results are shown in Figure 26. In this figure, the MOSES results are shown with wave steepness decreasing from 1/133 to 1/33. These wave steepnesses were chosen in order to correspond with those steepnesses tested by Noble Denton. The graph shows an agreement between test measurements and MOSES results.

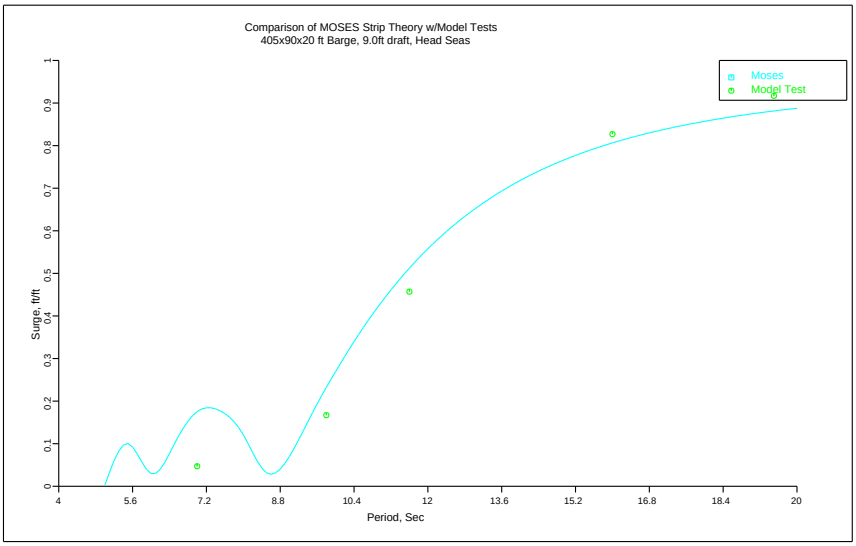

Figure 21: Comparison of Surge RAO in Head Seas

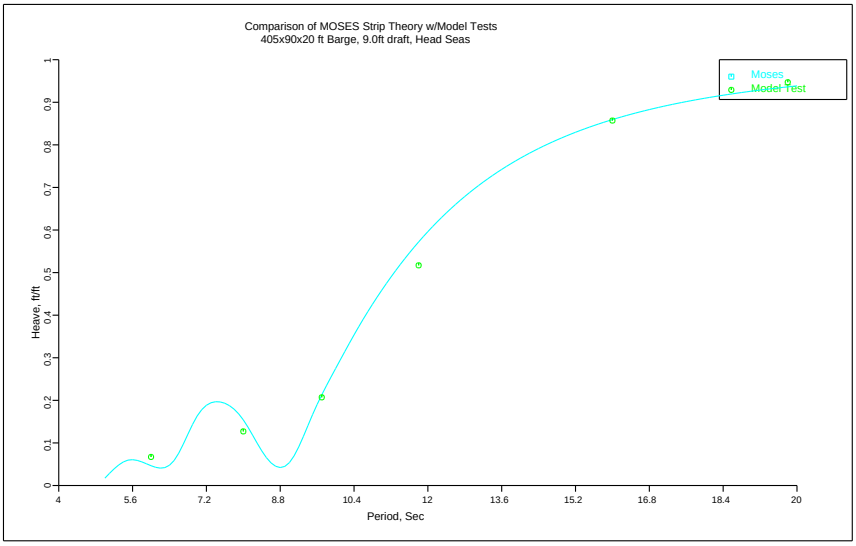

Figure 22: Comparison of Heave RAO in Head Seas

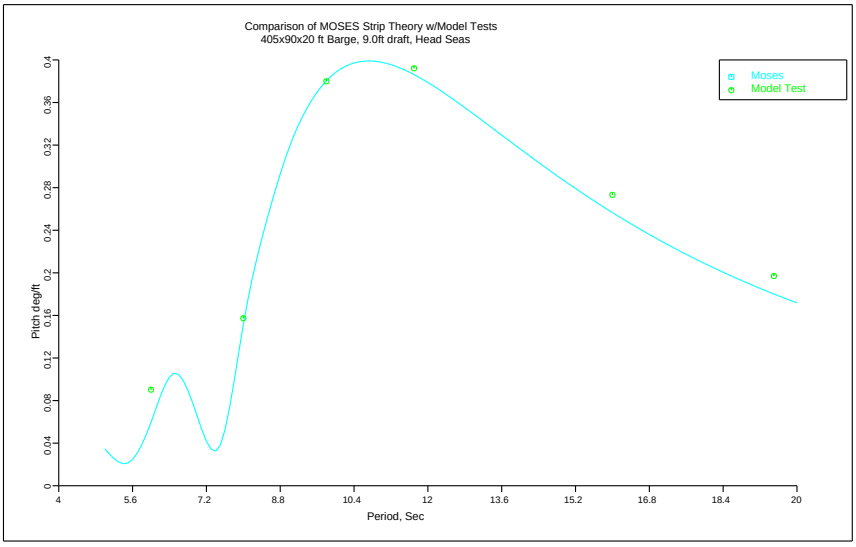

Figure 23: Comparison of Pitch RAO in Head Seas

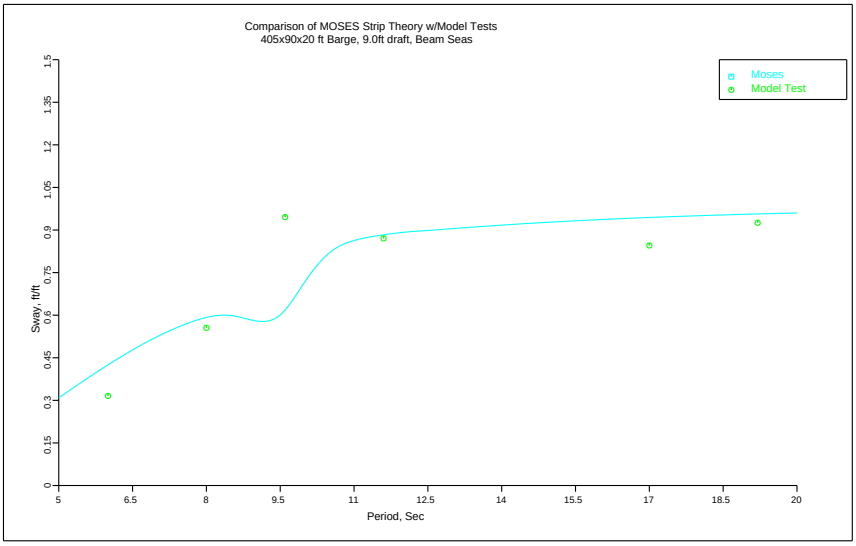

Figure 24: Comparison of Sway RAO in Beam Seas

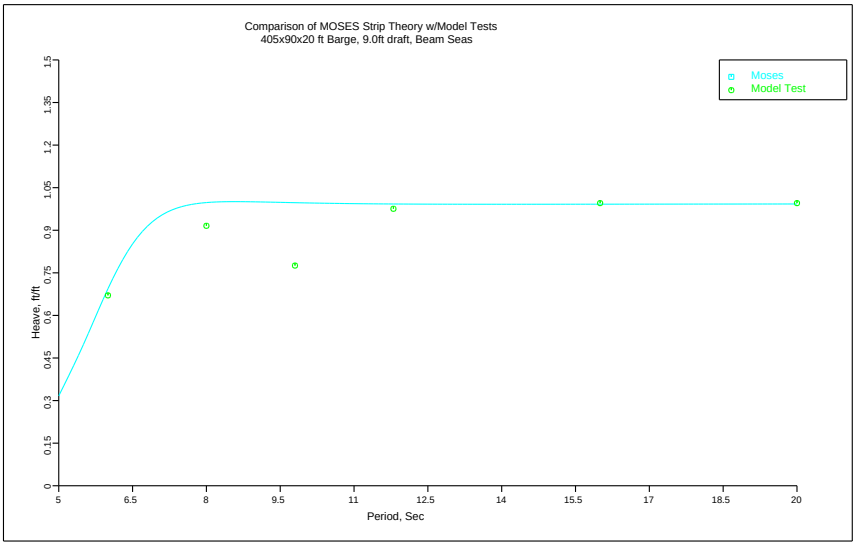

Figure 25: Comparison of Heave RAO in Beam Seas

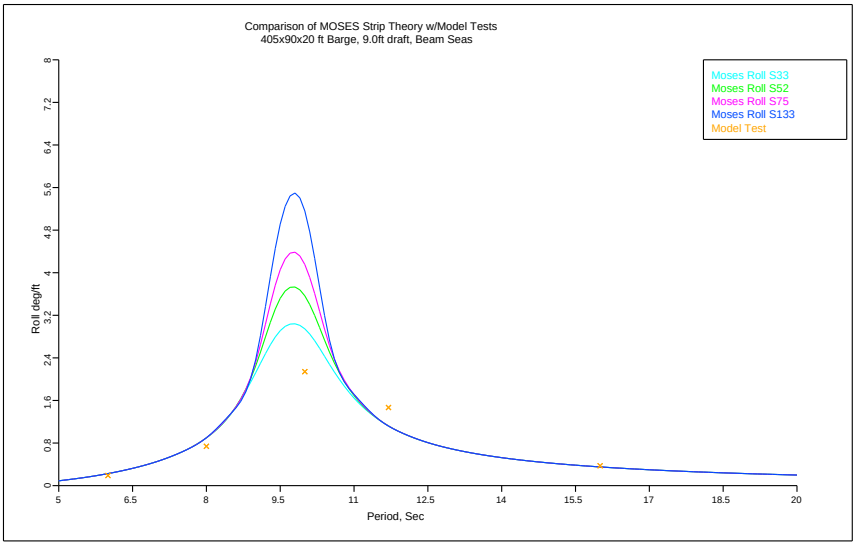

Figure 26: Comparison of Roll RAO in Beam Seas

XI. THREE DIMENSIONAL DIFFRACTION HYDRODYNAMICS

In this section, we will examine three dimensional diffraction results for semisubmersible vessel motions, comparing MOSES to the NSMB motions programs and to the model test results taken at NSMB [3]. It should be noted that NSMB, an acronym for Netherlands Ship Model Basin, is the former name for MARIN, Maritime Research Institute Netherlands.

The vessel used was the semisubmersible crane vessel Balder, with length, breadth and depth dimensions of 118 x 86 x 42 meters, respectively, at a 22.5 meter draft. Before comparison, the differences in the mathematical and test basin models should be noted. The displacement computed by MOSES was 3.3 percent greater than either NSMB model, and the MOSES KG was 1.87 meters lower than NSMB's. The KG shift was necessary in order to achieve equivalent transverse GM values. These indicate different values of waterplane inertia, which cannot be compared since they were not published in the NSMB report. Figures 27 illustrates the hydrostatic model used by MOSES.

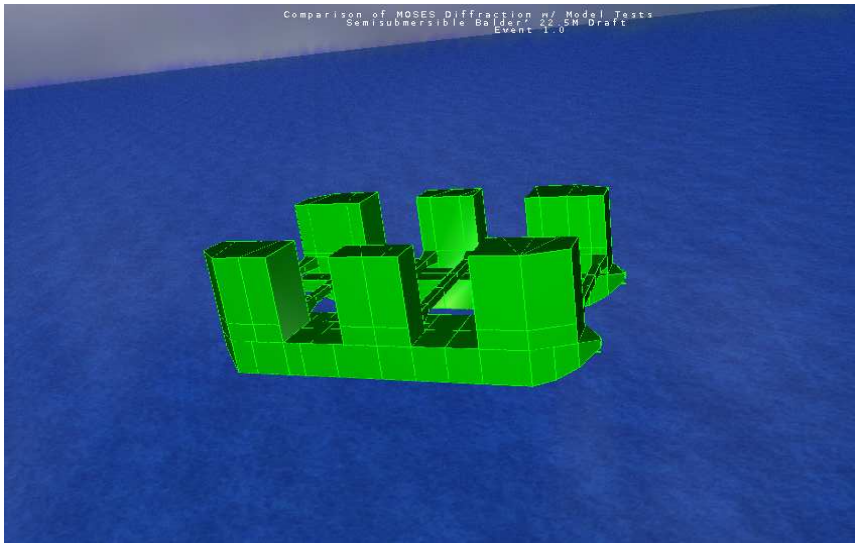

Figure 27: Isometric view of mesh model

This mesh was automatically refined by the program to generate a detailed mesh for

hydrodynamics, as seen in Figure 28 Imposing a constraint that the maximum panel side be less than four meters resulted in a diffraction mesh of 1130 panels. For the MOSES analysis, viscous damping was introduced by Morison tubular elements which attract only drag forces. Diameters for these tubulars were chosen to approximate the cross section of the pontoons and columns.

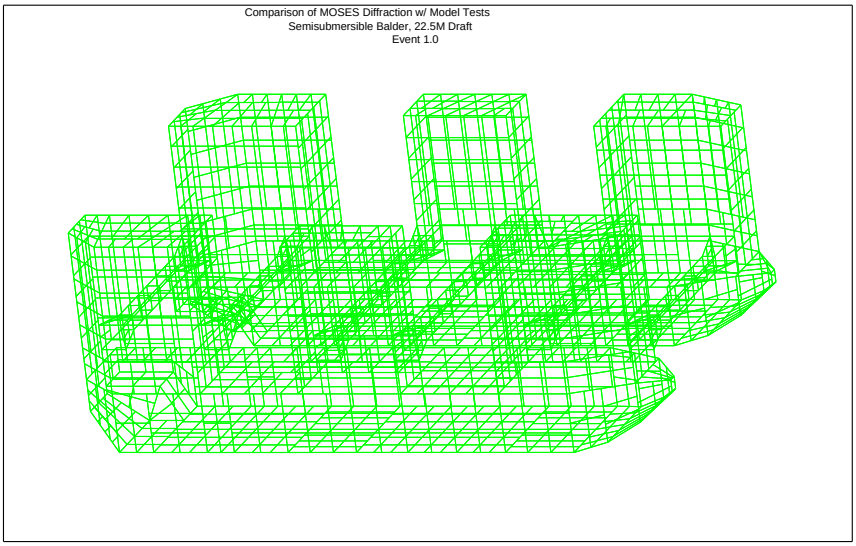

Figure 28: Isometric view of detailed mesh model

The response operators for head, quartering, and beam seas are shown in Figures 29 through 36 for periods up to 18 second. The legend in these figures label results from MOSES (MO), NSMB diffraction program (Nd) and NSMB model tests (Nt). The labels X, Y, Z, RX, RY refer to surge, sway, heave, roll and pitch, respectively, while the values of 180, 135 and 90 refer to head seas, quartering seas and beam seas. The agreement here is excellent.

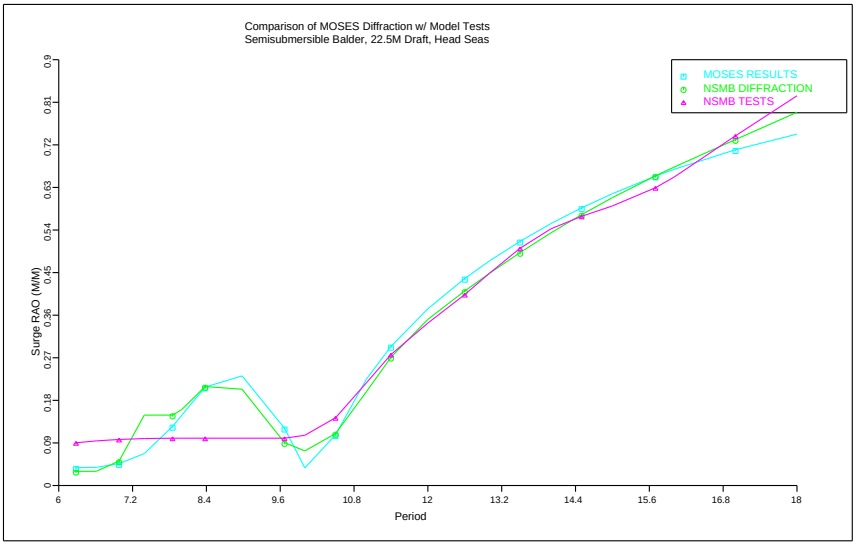

Figure 29: Surge comparison in head seas

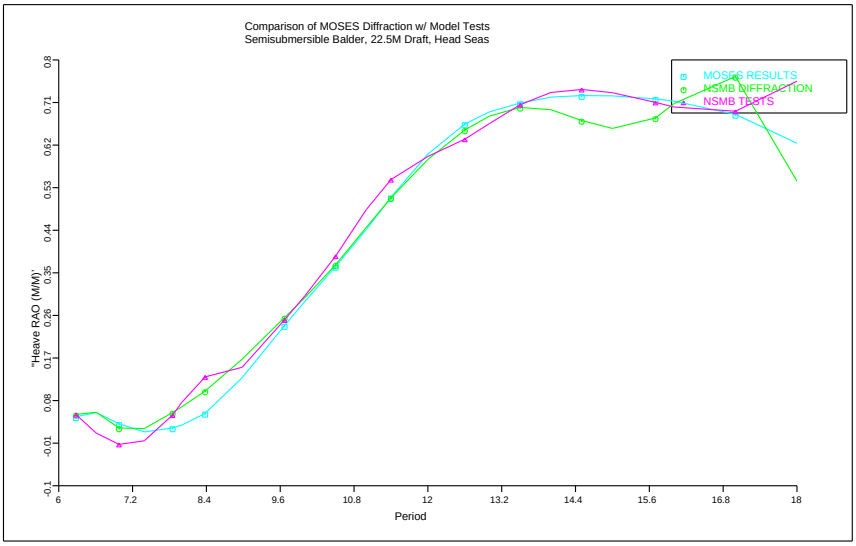

Figure 30: Heave comparison in head seas

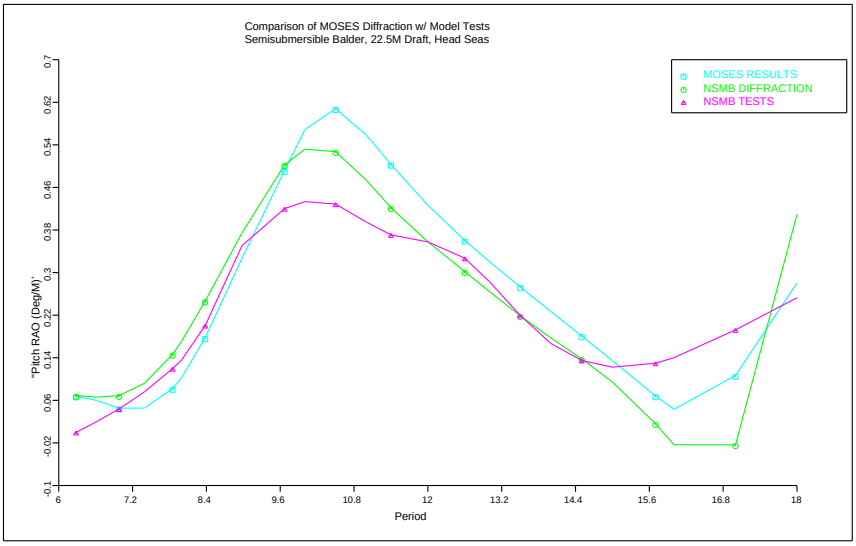

Figure 31: Pitch comparison in head seas

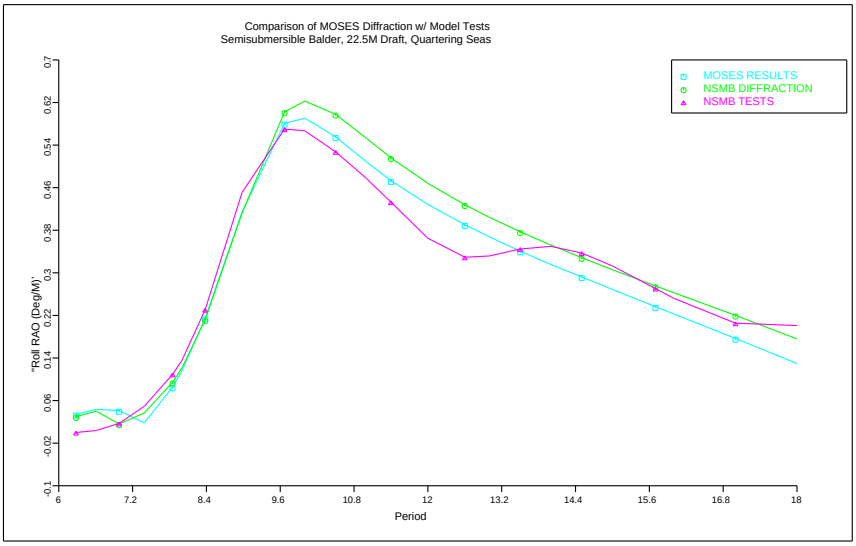

Figure 32: Roll comparison in quartering seas

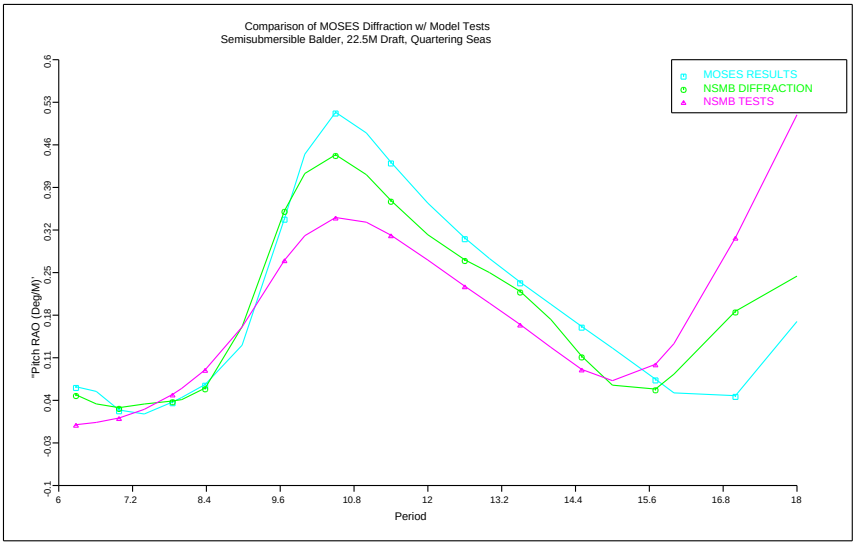

Figure 33: Pitch comparison in quartering seas

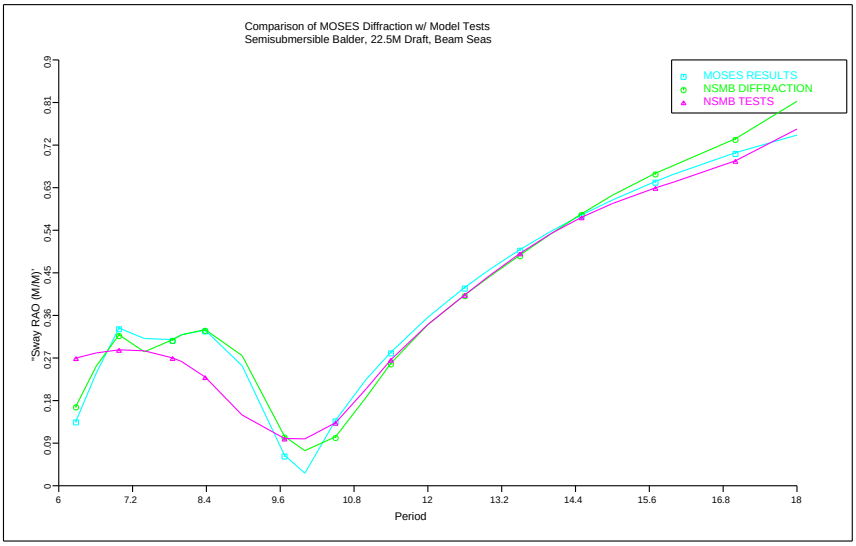

Figure 34: Sway comparison in beam seas

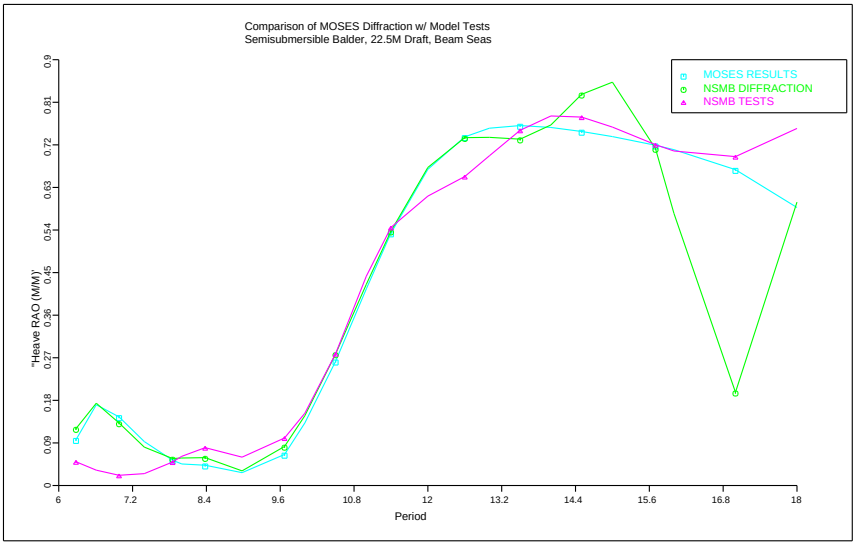

Figure 35: Heave comparison in beam seas

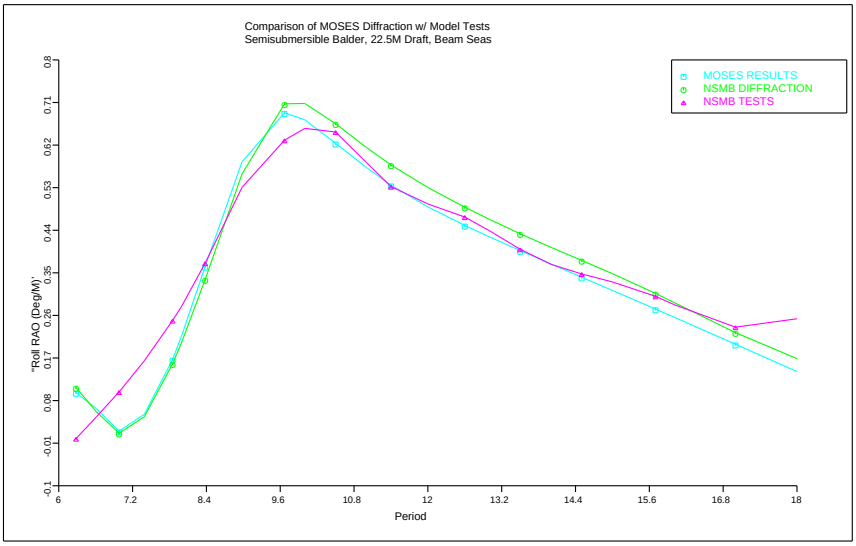

Figure 36: Roll comparison in beam seas

XII. HORIZONTAL OSCILLATION OF A TANKER

In this section, we compare MOSES predictions for the motions of a tanker on a single point mooring with those of Wichers [4]. The system consists of a ballasted 200 Kdwt tanker with a 90 m hawser connecting it to the single point. The SPM system is exposed to 60 knot head winds and a 1.03 m/sec. head current. The coordinate system used is shown in Figure 37. The global coordinate system is fixed to earth, and head seas are defined as the environment in the positive x-direction. Also shown in Figure 37 is the top view of the panel model used for the 200 Kdwt tanker.

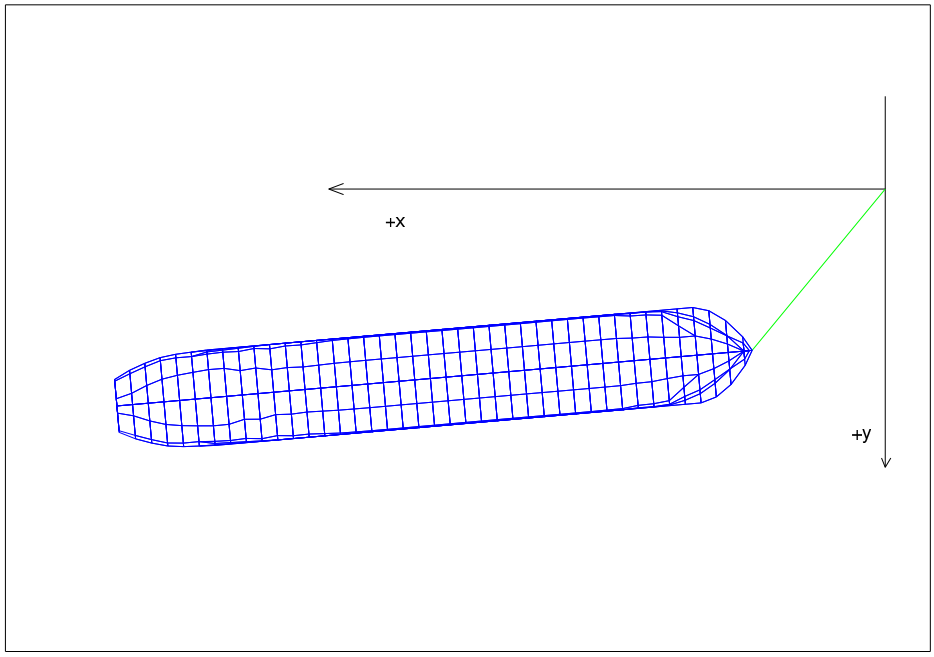

Figure 37: Coordinate system

The MOSES simulation consisted of 1700 sec. at 2 sec. intervals. Figures 38 and 39 show the x and y motions vs. time for: the model tests, the simulation conducted by Dr. Wichers, and the MOSES simulation. These results are quite interesting in that we have an unsteady motion of the system in an environment which is constant. In other words, what we see here is the result of an instability. In view of this, the closeness of the three results is quite remarkable. Wichers used experimental results to obtain coefficients in his simulation. For the MOSES simulation, the wind and current forces were computed using the #tanker load group and nothing else was done.

Perhaps of even greater interest here is the variation of the tanker yaw angle with

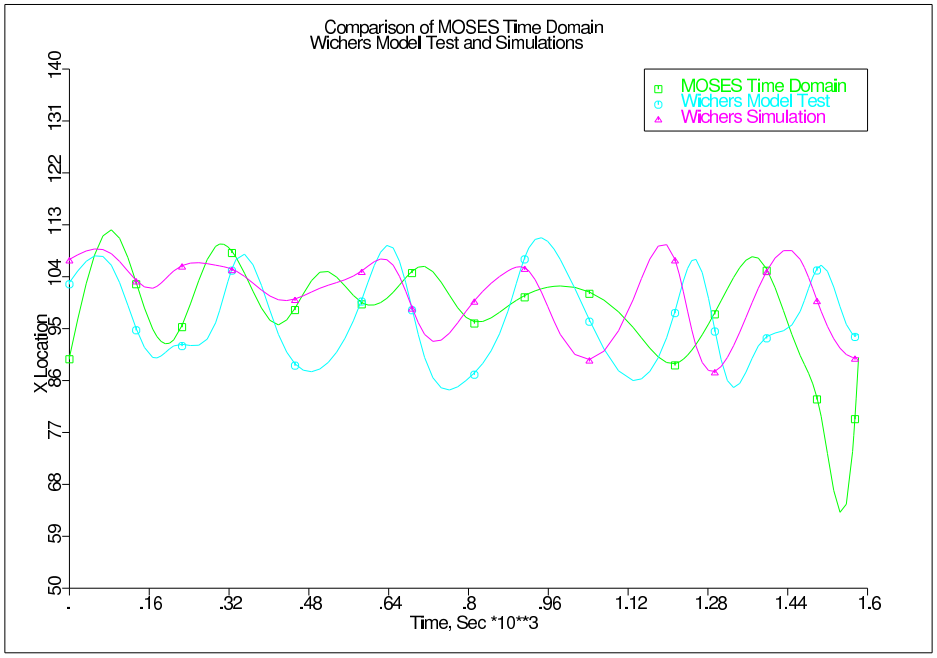

Figure 38: Comparison of x motions

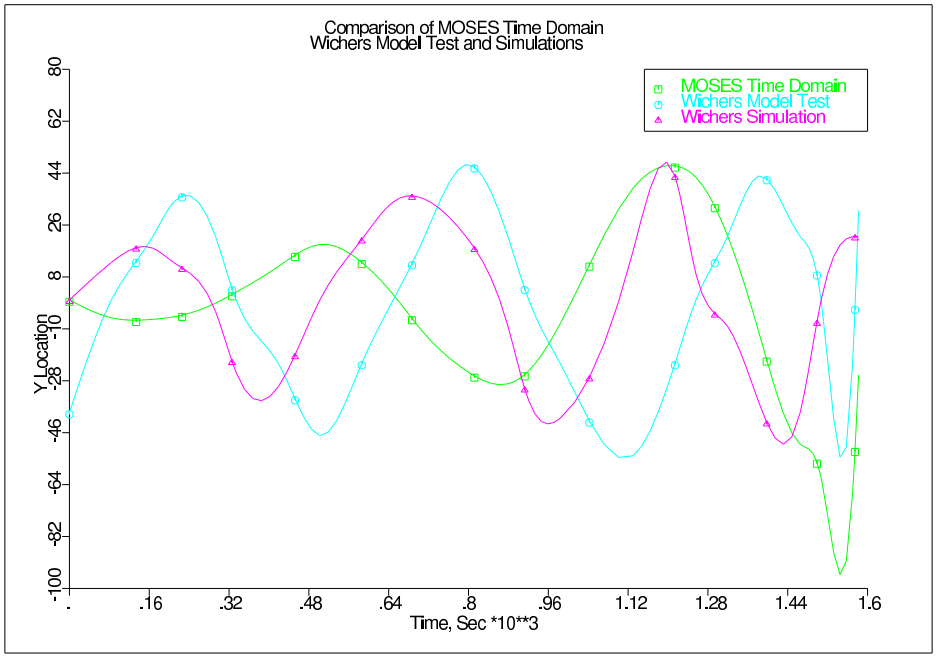

Figure 39: Comparison of y motions

time. This is shown in Figure 40.

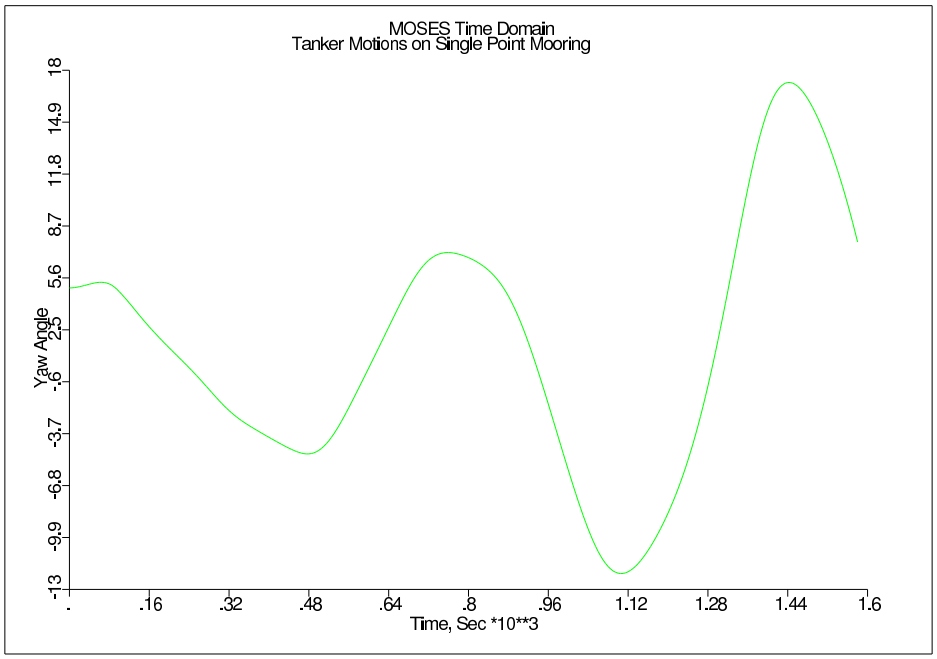

Figure 40: Yaw motion for Single point mooring

XIII. WIND AND CURRENT FORCE

In this section, we consider the ways in which MOSES computes wind and current forces. In essence, there are five ways: Morrison's Equation for a tube (#TUBE), Morrison's Equation for a plate (#PLATE), using the panels of a "Piece" (closed surface producing buoyancy and hydrodynamics), #TABLE, and #TANKER. The mathematics of computing the force for the first three load attractors is the same for wind and for current and for each of the elements. The only difference is in how the "drag coefficient" vector is defined. In what follows we will use a vector $\boldsymbol{c}$ which, in general, can be defined as:

$$\boldsymbol{c} = (C_x, C_y, C_z) \tag{XIII.1}$$

For both plates and tubes, all values are the same and are specified with a MOSES &PARAMTER setting. For tubes, the coefficients for wind forces are specified with -WCSTUBE and for water forces with a Reynolds' number dependent table specified with -DRGTUB. For plates, it is specified with -DRGPLA for both wind and water. For panels, these are defined with the options -CS_WIND and -CS_CURR on either the PGEN or PIECE command.

The force on each panel is computed as

$$\boldsymbol{f} = sqA\boldsymbol{e} \tag{XIII.2}$$

Where $\boldsymbol{f}$ is the force vector, $\boldsymbol{e}$ is a unit vector, $\boldsymbol{r}$ is the relative velocity vector , A is the area, and s and q are multipliers. Here s is given by

$$s = .5\rho \parallel \boldsymbol{r} \parallel \tag{XIII.3}$$

where ρ is the density of of the fluid, and the last term is the relative speed. The multiplier q is given by

$$q = \sum_i [c(i)n(i)r(i)] \tag{XIII.4}$$

where $\boldsymbol{n}$ is the normal to the area and $c(i)$ are the components of the $\boldsymbol{c}$ vector.

The meaning of A and $\boldsymbol{e}$ depend on the current setting of a MOSES parameter specified with -AF_ENVIRONMENT. If you use YES then

$$\begin{aligned} \boldsymbol{e} &= \boldsymbol{r} / \parallel \boldsymbol{r} \parallel \\ A &= a(\boldsymbol{n} \cdot \boldsymbol{r}) / \parallel \boldsymbol{r} \parallel \end{aligned} \tag{XIII.5}$$

where a is the area of the panel or diameter times the length of a tube. If NO was used, then

$$\begin{aligned} \boldsymbol{e} &= \boldsymbol{n} \\ A &= a \end{aligned} \tag{XIII.6}$$

his means the in the first case the force will be in the direction of the relative velocity while in the second it is normal to the area.

To see how the forces on panels works, we looked at the forces on the three shapes shown in Figure 41.

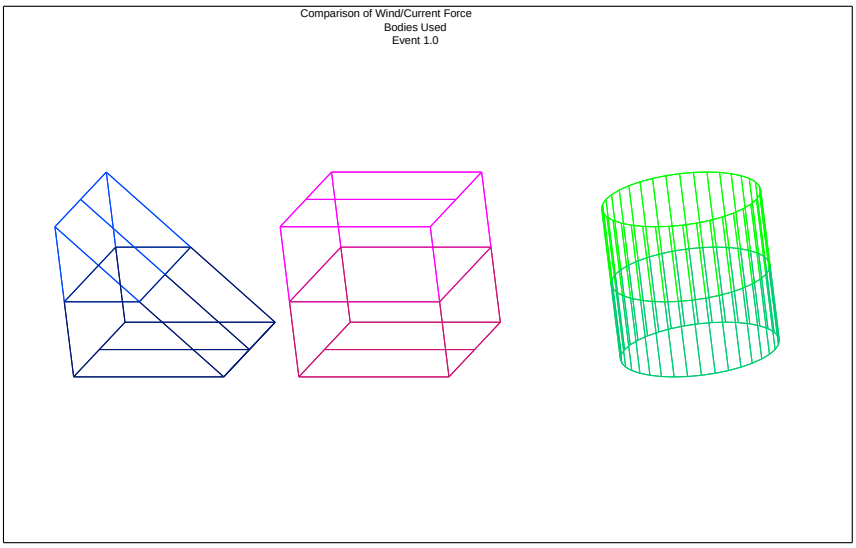

Figure 41: Definitions of Shapes

Figures 42 - 44 show the surge, sway, current force and the magnitude of the force ($\| \boldsymbol{f} \|$) on each of the shapes. Here, the force is computed using the MOSES Method, -AF_ENVIRONMENT NO.

The thing to notice here is that the force depends on the shape; i.e. by integrating the force over the the body you get a dependence of the force on the shape of the piece. For head and beam currents, one gets a force of $\pi/4$ times that of the square. Thus if you want half that of a square you need to specify .5/.785 for the for C_x and C_y.

One should notice that the directional behavior for the wind is identical to the current so only one of them is presented here. Now, notice that the magnitude of the force on both the tube and the square are independent of angle. This is a direct result of the fact that the x and y projected areas are the same and the force computation method. Figures 45 compares the magnitude of the force for the two computation

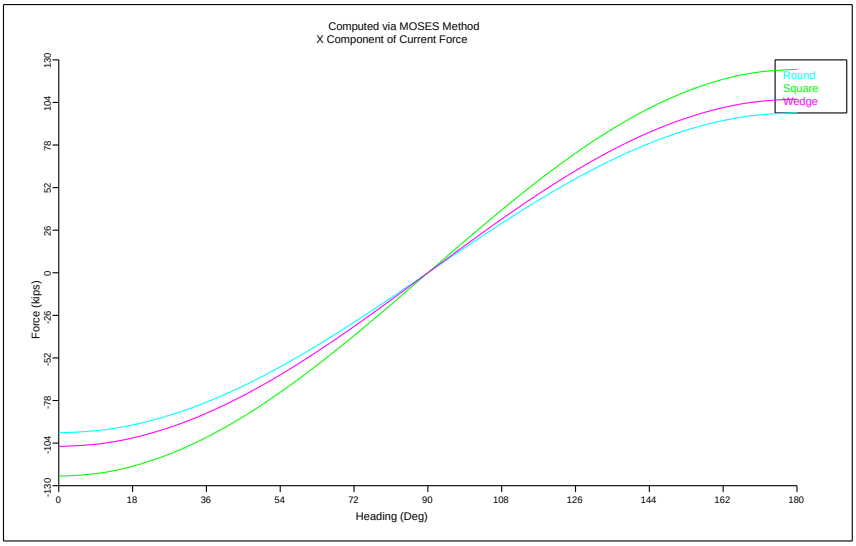

Figure 42: Current Surge Force

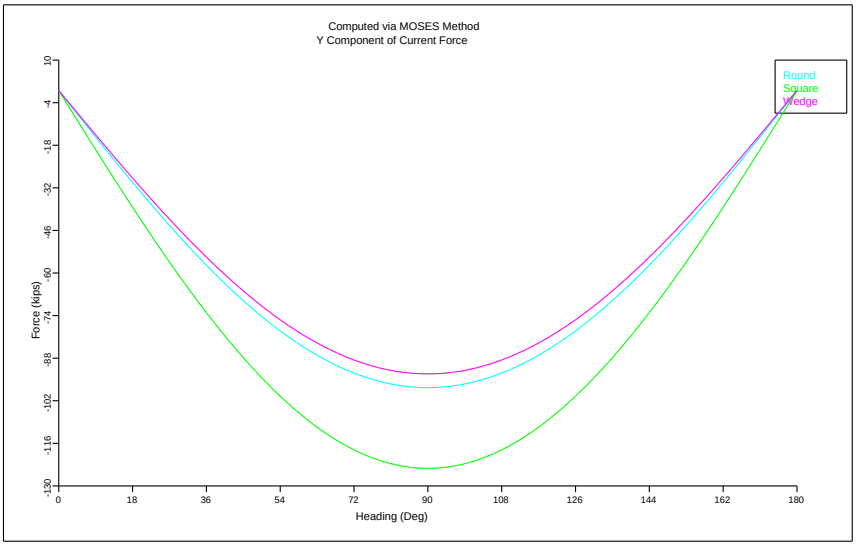

Figure 43: Current Sway Force

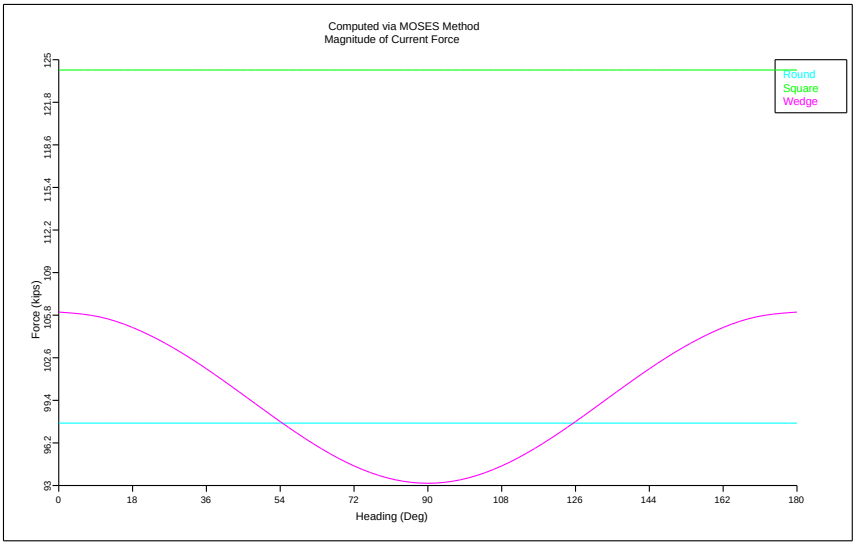

Figure 44: Current Force Magnitude

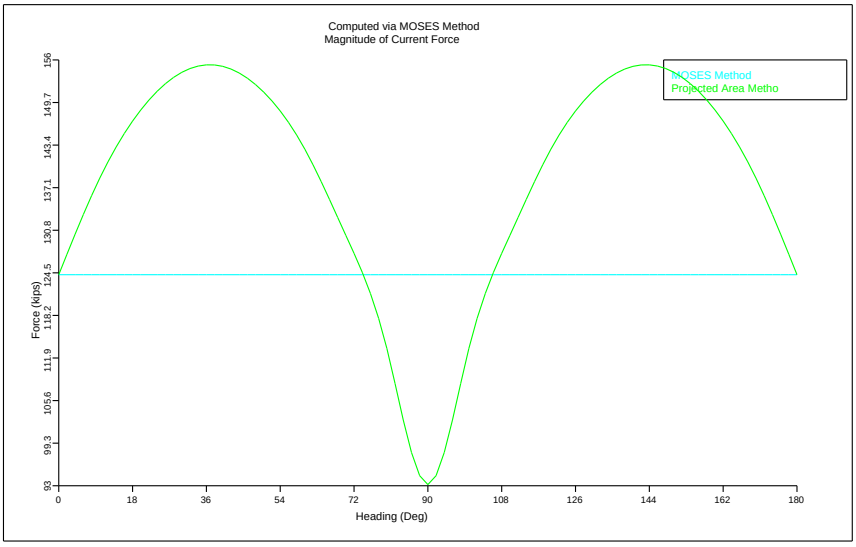

Figure 45: Current Force Magnitude By Method

methods.

Here one can see that the "projected area" method produces a larger force for headings other than head or beam, but it does not take into account that the "drag" coefficient is different for a wedge than for a flat surface.

We have been discussing these forces in the context of regulatory "recepies". In other words, the mathematics above is consistent with traditional "rules" such as ABS, API, or DNV. The next three figures Figures 46 - 48 show comparisions of the surge, sway, and yaw forces on a tanker computed by #TANKER and by the panel integration method. The #TANKER method is based on the data published by published by OCIMF [2] which was based on model tests.

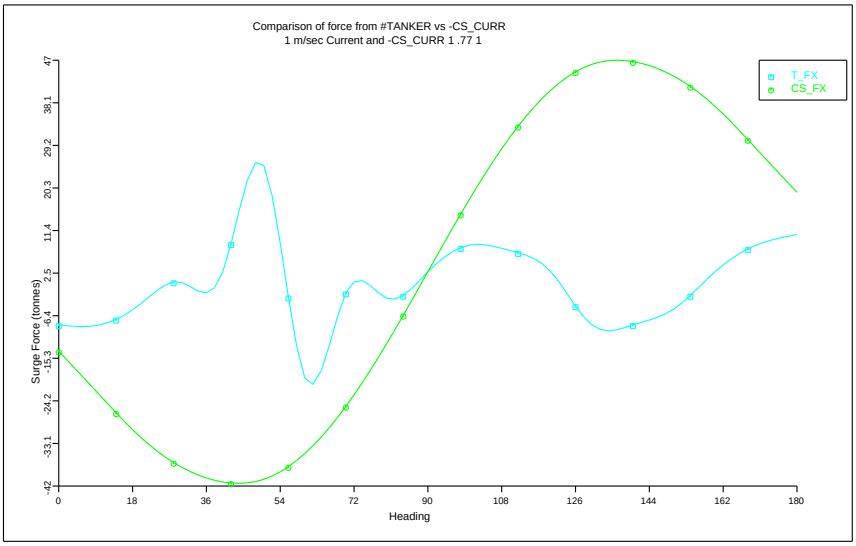

Figure 46: Comparision of Tanker Current Surge

The interesting thing here is that while the surge force comparison is quite poor, the comparison for the other two components is quite reasonable. This simply demonstrates that it is not realistic to expect to capture complex interaction with a simple

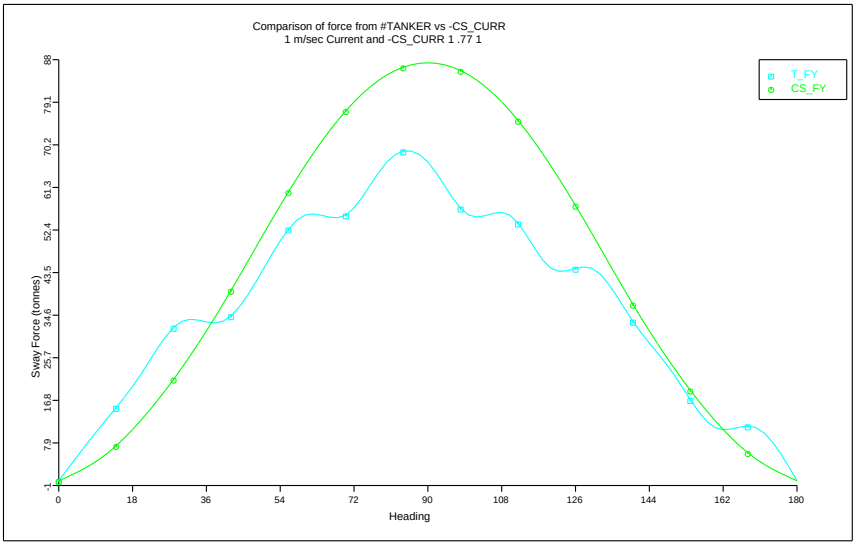

Figure 47: Comparision of Tanker Current Sway

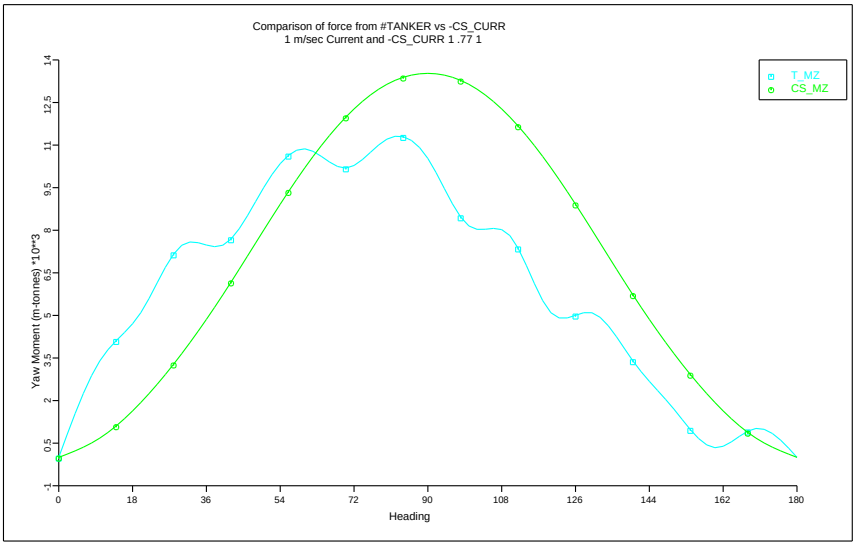

Figure 48: Comparision of Tanker Current Yaw

receipe.

While we have been talking about "current force", the forumlae depend on the relative velocity. As a result, we should expect some damping to be produced. Figures 49 - 53 show examples of the damping produced by the panel integration "current" force computation.

Figure 49 shows a comparison of the roll response of a barge for two values of wave steepness (the same case considered in Section IX above). In one case, we have only Tanaka damping while in the other we have only damping produced by the panel integration method. The comparison here is remarkable. This is especially true since the "Tanaka" damping is supposed to be a result of eddy formation at the bilge and the panel integration is simply due to pressure drag over the bottom. This is quite important. It says that if one uses panel integration to capture current force, then he should either set C_z to zero or set other roll damping to zero.

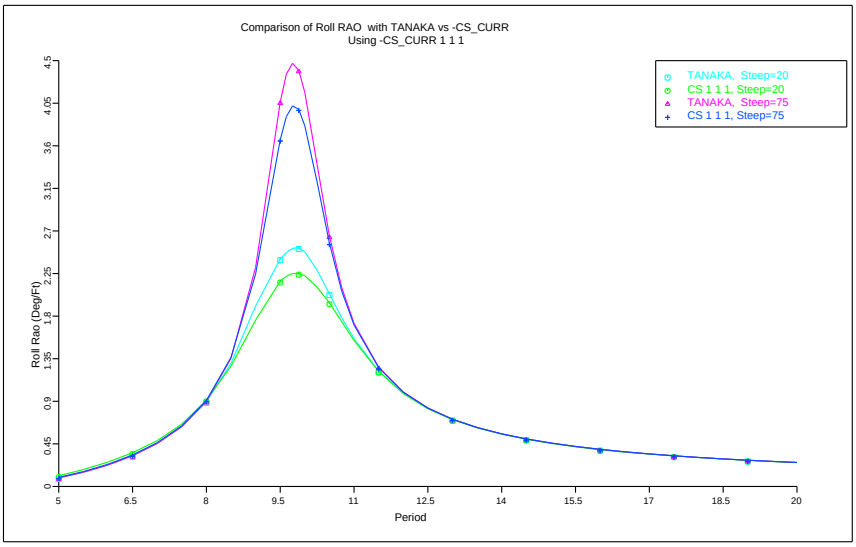

Figure 49: Comparision of Damping with TANAKA

Figure 50 and figure 51 show a comparison of the heave and roll response of the BALDER (same condition as that reported in Section X above) using #TUBE for damping and using the panel integration method. Again, the agreement is excellent and the panel integration method does not require defining any "special" elements.

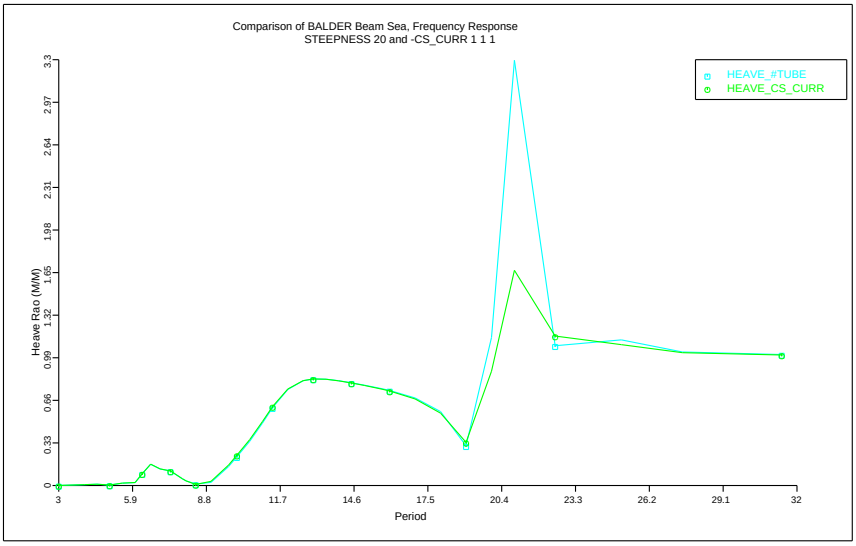

Figure 50: Comparison of Damping with #TUBE in Heave

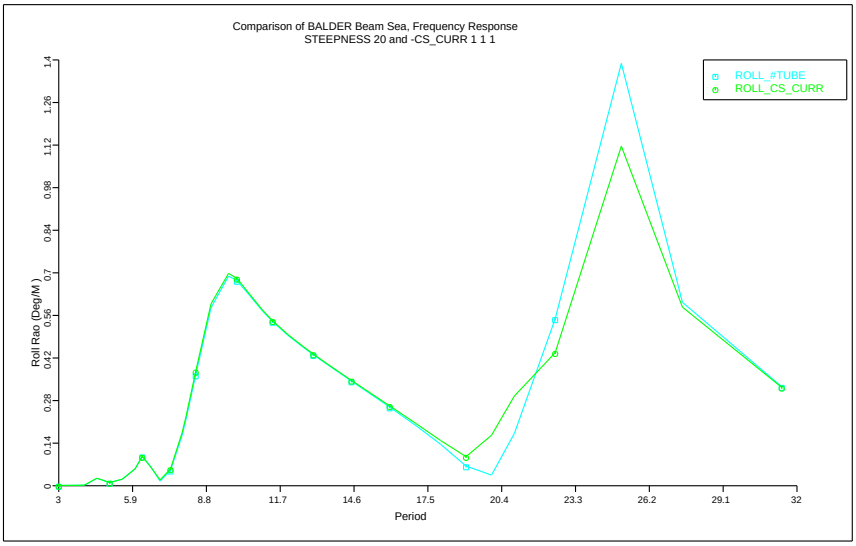

Figure 51: Comparison of Damping with #TUBE in Roll

Finally, figure 53 shows a comparison of the heave decay of the BALDER with computed panel integration damping, computed with 3% critical damping, and Model Tests. Again the comparison is quite good with the model tests showing more damping than the other two methods.

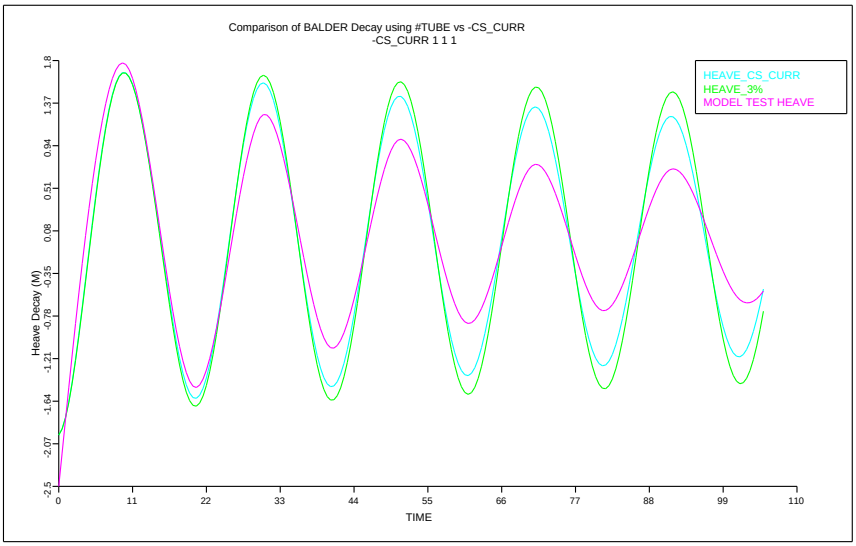

Figure 52: Heave Decay

XIV. PIPELAYING

In this section, we will consider the results of a static pipelaying analysis. In particular, will will compare the results from MOSES to those of the OFFPIPE program. The pipe used here is a steel pipe, 12 inches diameter, 0.75 inch thickness, laid in 1600 meters of waterdepth. The figure 53 shows both the axial force and bending moment along the pipe resulting from each program. The two sets of curves agree well except for the moment between 2800 meters and 2970 meters. This is probably due to the fact that OFFPIPE's results used a nonlinear moment-curvature relationship while MOSES used linear ones.

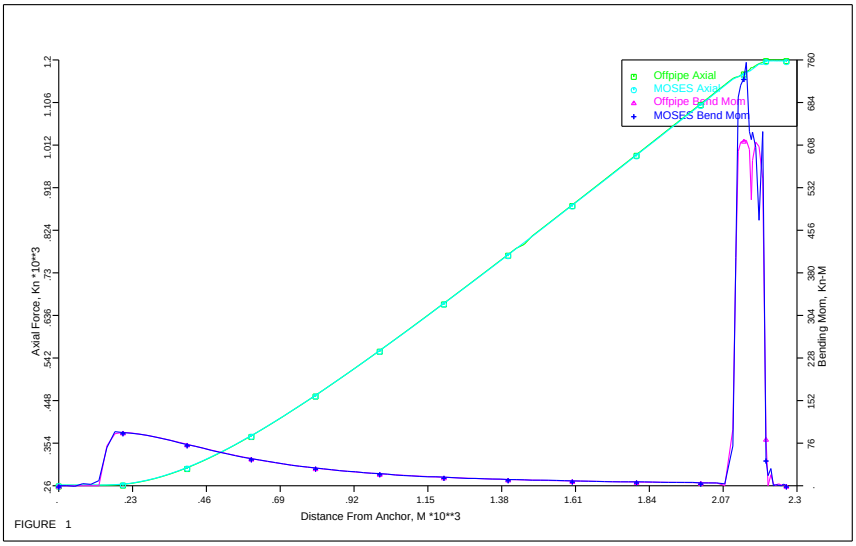

Figure 53: Comparison of axial force and bending moment along the pipe

References

[1] *Barge Motions Research Project*, Phase 1 Report, for a consortium of companies organised by Noble Denton and Associates Ltd., December 1978.

[2] *Prediction of Wind and Current Loads on VLCCs* by the Oil Companies International Forum (OCIMF).

[3] Netherlands Ship Model Basin Report No. 45065-1-ZT, *The Damping Controlled Response of Semi-submersibles* Wageningen, February, 1984.

[4] Wichers, J.E.W., "The Prediction of the Behaviour of Single Point Moored Tankers", *Floating Structures and Offshore Operation* , Elsevier Place, Oxford, 1988.